

PHENOMENOLOGY OF LEP 2 PHYSICS**John ELLIS**Theoretical Physics Division, CERN
CH - 1211 Geneva 23**ABSTRACT**

Various aspects of physics at LEP 2 are reviewed from a phenomenological point of view. We first discuss the search for Higgs bosons, which might be relatively light if indications from precision electroweak data and supersymmetry are correct. Then WW physics is discussed, with particular emphasis on the problems in measuring m_W by the kinematic reconstruction of events with purely hadronic final states. Finally, possible manifestations of supersymmetry are reviewed, comparing different scenarios for the lightest supersymmetric particle, which may or may not be stable. Possible scenarios for R violation at HERA and future searches for supersymmetry at the LHC are also mentioned briefly.

*Lectures presented at the Lake Louise Winter Institute
Lake Louise, Alberta, Canada
February 1997*

CERN-TH/97-131
July 1997

PHENOMENOLOGY OF LEP 2 PHYSICS

John Ellis

*Theoretical Physics Division, CERN
CH - 1211 Geneva 23*

Various aspects of physics at LEP 2 are reviewed from a phenomenological point of view. We first discuss the search for Higgs bosons, which might be relatively light if indications from the precision electroweak data and supersymmetry are correct. Then WW physics is discussed, with particular emphasis on the problems in measuring m_W by the kinematic reconstruction of events with purely hadronic final states. Finally, possible manifestations of supersymmetry are reviewed, comparing different scenarios for the lightest supersymmetric particle, which may or may not be stable. Possible scenarios for R violation at HERA and future searches for supersymmetry at the LHC are also mentioned briefly.

Preamble

The cross-sections for the most important physics processes that we expect (or hope) to see at LEP 2 are shown in Fig. 1¹. The reactions $e^+e^- \rightarrow \bar{f}f$, which have been the bread and butter of LEP 1 physics, become backgrounds to be fought at LEP 2. The reaction $e^+e^- \rightarrow W^+W^-$ is likely to provide the new bread and butter for LEP 2. The reaction $e^+e^- \rightarrow Z^0Z^0$ has not excited much interest so far, though it may provide a pesky background to the Higgs search if $M_H \sim 90$ GeV. We can but hope that the reaction $e^+e^- \rightarrow Z + H$ ² is accessible to LEP 2!

The upgrades of LEP using superconducting RF cavities started in the Autumn of 1995 with the first runs at $E_{cm} = 130$ and 136 GeV, and a little data at 140 GeV, known collectively as LEP 1.5^a. These were followed in the Summer of 1996 by the first runs above the W^+W^- threshold, at $E_{cm} = 161.3$ GeV, known as LEP 2W. Later in 1996 came runs at 170/172 GeV referred to here as LEP 2. Cross-sections for $e^+e^- \rightarrow \bar{f}f$ measured at LEP 1, 1.5, 2W and 2 energies are shown in Fig. 2³. Subsequent plans include runs at $E_{cm} \simeq 184$ GeV during 1997, and at $E_{cm} \simeq 192$ GeV in 1998 and 1999. There is a possibility of increasing the maximum LEP 2 energy to about 200 GeV if the superconducting RF can be coaxed to higher accelerating fields ~ 7 MeV/m

^aSince $E_{cm} \simeq 1.5m_Z$.

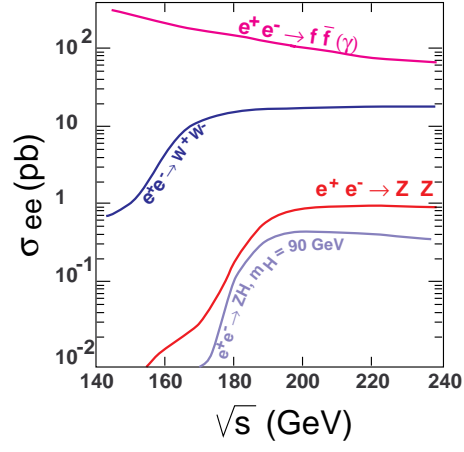


Figure 1: Cross-sections for the main processes to be measured at LEP 2.

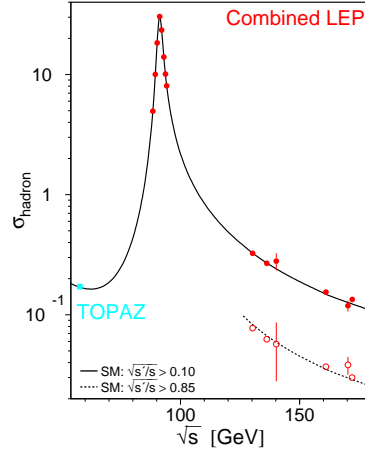


Figure 2: Measured e^+e^- hadron cross-sections at LEP and from the lower-energy TOPAZ experiment at KEK. At high energies, the measured cross-section depends strongly on the cut on the observed energy $\sqrt{s'}$ that is imposed.

with the aid of the LHC cryogenics system. Running LEP in the year 2000 also seems to be compatible with the LHC construction schedule, though this will cause earth motion that may complicate LEP running from 1999 onwards. It remains to be seen whether physics will warrant, and finances permit, running LEP during the year 2000. But enough of this preamble: now is the time to address the first item on the physics agenda for LEP 2.

1 In pursuit of the Higgs boson

1.1 Precision Electroweak Measurements

These are available from a large range of energies and distance scales, extending from parity violation in atoms through various fixed-target lepton scattering experiments to high-energy experiments at e^+e^- , $\bar{p}p$ and ep colliders. Among these, the largest weight is currently carried by the e^+e^- experiments at the Z^0 peak at LEP and the SLC, together with the Tevatron collider experiments CDF and $D0$. The high- Q^2 events from HERA^{4,5} are another story ...

The basic measurements on the Z^0 peak⁶ include the total hadronic cross-section, which is given at the tree level by

$$\sigma_h^0 = \frac{12\pi}{m_Z^2} \frac{\Gamma_{ee}\Gamma_{had}}{\Gamma_Z^2} \quad (1.1)$$

which is reduced substantially by radiative corrections (principally Initial-State Radiation, ISR) to about 30 nb. The total Z decay rate may be decomposed as

$$\Gamma_Z = \Gamma_\ell + \Gamma_\mu + \Gamma_\tau + \Gamma_{had} + N_\nu \Gamma_\nu \quad (1.2)$$

where all the data are consistent with the lepton universality expected in the Standard Model: $\Gamma_e = \Gamma_\mu = \Gamma_\tau \equiv \Gamma_\ell$, which also predicts $\Gamma_\nu = 1.991 \pm 0.001\Gamma_\ell$. We parametrize the total decay rate of the Z^0 into invisible particles as $\Gamma_{inv} = N_\nu \Gamma_\nu$. The partial decay rate for leptons is often parametrized as $R_\ell \equiv \Gamma_{had}/\Gamma_\ell$, and the Z^0 decays into heavier quarks by $R_{b,c} \equiv \Gamma_{b,c}/\Gamma_{had}$.

Other precision measurements on the Z^0 peak⁶ include forward-backward asymmetries A_{FB} : at the tree level for $f \neq e$:

$$\frac{d\sigma}{d\cos\theta} (e^+e^- \rightarrow \bar{f}f) \simeq (1 + \cos^2\theta) F_1 + 2\cos\theta F_2 \quad (1.3)$$

and

$$A_{FB} = \frac{\left(\int_0^1 - \int_{-1}^0\right) d\cos\theta \cdot \frac{d\sigma}{d(\cos\theta)}}{\int_{-1}^1 d\cos\theta \cdot \frac{d\sigma}{d(\cos\theta)}} = \frac{3F_2}{4F_1} \quad (1.4)$$

which takes the value $A_{FB} = \frac{3}{4}(1 - 4\sin^2\theta_W)^2$ for $\mu^+\mu^-$ and $\tau^+\tau^-$ in the Standard Model. Also of interest is the final-state τ polarization

$$P_\tau = \frac{2(1 - 4\sin^2\theta_W)}{1 + (1 - 4\sin^2\theta_W)} \quad (1.5)$$

at the tree level in the Standard Model, whose different functional dependence on $\sin^2\theta_W$ gives it greater sensitivity. Of particular interest at the SLC is the difference between the cross-sections for left- and right-handed electron beams, the polarized-beam asymmetry

$$A_{LR} = \frac{\sigma_L - \sigma_R}{\sigma_L + \sigma_R} = \frac{2(1 - 4\sin^2\theta_W)}{1 + (1 - 4\sin^2\theta_W)^2} \quad (1.6)$$

at the tree level. Clearly, this requires a longitudinally-polarized beam, which SLAC has available, whereas LEP only has transversely-polarized beams, whose utility will become apparent shortly.

Table 1 includes a summary³ of the current status of all these key precision electroweak measurements, among others including the measurements of m_W , which are denominated by those at FNAL⁸. We note in particular the effective number of light neutrino species

$$N_\nu = 2.992 \pm 0.011 \quad (1.7)$$

which is an important piece of information for cosmological nucleosynthesis, discussed here by Keith Olive⁷. Some of the fun physics involved in the precise determination of M_Z and Γ_Z merits further discussion.

It has been known for some years that the LEP beam energy is sensitive to terrestrial tides⁹. These cause the rock in which LEP is embedded to rise and fall by about 25 cm each day, inducing variations in the LEP circumference $\Delta C \simeq 1$ mm. Because the angular rotational velocity of the beams is fixed by the frequency of the RF system, the beams are forced to change trajectory so as to “cut corners” when LEP expands, which induces a fractional change in energy $\Delta E/E \simeq 10^{-4}$. This tidal effect can be predicted quite reliably, and measurements of the LEP beam energy, using resonant depolarization of the transversely-polarized beams, agree well with the predictions of the tidal

Table 1:

	Measurement		
m_Z [GeV]	91.1863	\pm	0.0019
Γ_Z [GeV]	2.4947	\pm	0.0026
σ_{had}^0 [nb]	41.489	\pm	0.055
R_1	20.783	\pm	0.029
$A_{fb}^{0,1}$	0.0177	\pm	0.0010
A_τ	0.1401	\pm	0.0067
A_e	0.1382	\pm	0.0076
$\sin^2 \theta_{eff}^{lept}$	0.2322	\pm	0.0010
R_b	0.2177	\pm	0.0011
R_c	0.1722	\pm	0.0053
$A_{fb}^{0,b}$	0.0985	\pm	0.0022
$A_{fb}^{0,c}$	0.0735	\pm	0.0048
A_b	0.897	\pm	0.0047
A_c	0.623	\pm	0.085
$\sin^2 \theta_{eff}^{lept}$	0.23055	\pm	0.00041
$1 - m_W^2/m_Z^2$	0.2244	\pm	0.0042
m_W [GeV]	80.37	\pm	0.08
m_t [GeV]	175.6	\pm	5.5

model, as seen in Fig. 3a. Since these variations in the beam energy are of order 10 MeV, they need to be taken into account in order to extract m_Z , whose quoted error of about 2 MeV³ is much smaller.

To arrive at this precision, very careful monitoring of the LEP beam energy is necessary, and several other bizarre effects have shown up. Figure 3b shows variations in the length of one arc of LEP, which is correlated with the beam energy by the “corner-cutting” effect mentioned above. As can be seen in Fig. 3b, a large part of the variation in 1993 is correlated with the height of the water table in the Jura mountains. This is understandable, since the rock expands as it absorbs more water. However, this is not the whole story. There is also a correlation with changes in the water level of Lake Geneva¹⁰, as seen in Fig. 3c. This reflects the fact that water is run off during the first part of the year to make room in the Spring for molten snow from the mountains. With the weight of the water removed, the bedrock rises on a time scale of

about 100 days^b, causing LEP to expand and its energy to vary.

In principle, beam energy calibration using resonant depolarization during the LEP fill monitors all these effects so that they no longer affect the determination of m_Z . However, more recently it has been discovered that the beam energy varies systematically during a fill, which is problematic in view of the fact that the beam energy is typically calibrated at the end of a fill. This variation is least important during the night. After some puzzlement, during which possible sources of electrical interference were sought on the CERN site, the origin was finally identified as trains on the nearby railway line between Geneva and France¹¹, as seen in Fig. 3d. The interpretation is that some current leaks from the rails through the earth (which is not a perfect insulator) and particularly the LEP ring (which is a much better conductor), before returning to the rails via the Versoix river. This varying current perturbs the LEP magnets, which settle into a domain configuration with slightly higher field, and hence beam energy, as can be seen in Fig. 3d. This effect is potentially larger than the quoted error on m_Z and has had to be taken into account. Figure 4 tabulates the latest determinations of m_Z by the four LEP collaborations³, including this “TGV effect”.

What is the significance of this measurement? At the tree level, in the Standard Model one has

$$m_Z = \sqrt{\frac{\pi\alpha}{\sqrt{2}G_\mu}} \frac{1}{\sin\theta_W \cos\theta_W} \quad (1.8)$$

where $\sin^2\theta_W$ is related to the ratio of gauge boson couplings:

$$\sin^2\theta_W = \frac{g'^2}{g'^2 + g_2^2} \quad (1.9)$$

whose value is a key discriminant between different grand unified theories. The error in m_Z is now comparable to that in the μ decay constant G_μ . The value of the fine-structure constant α is well known in the low-energy Thomson limit, but the value most relevant to m_Z is that at high energies, which is modified by radiative corrections. These are sensitive to virtual particles such as the top quark and our quarry in this lecture, the Higgs boson, whose effects we discuss in the next section.

^bFor comparison, we recall that the North of Canada is still rising after the last Ice Age.

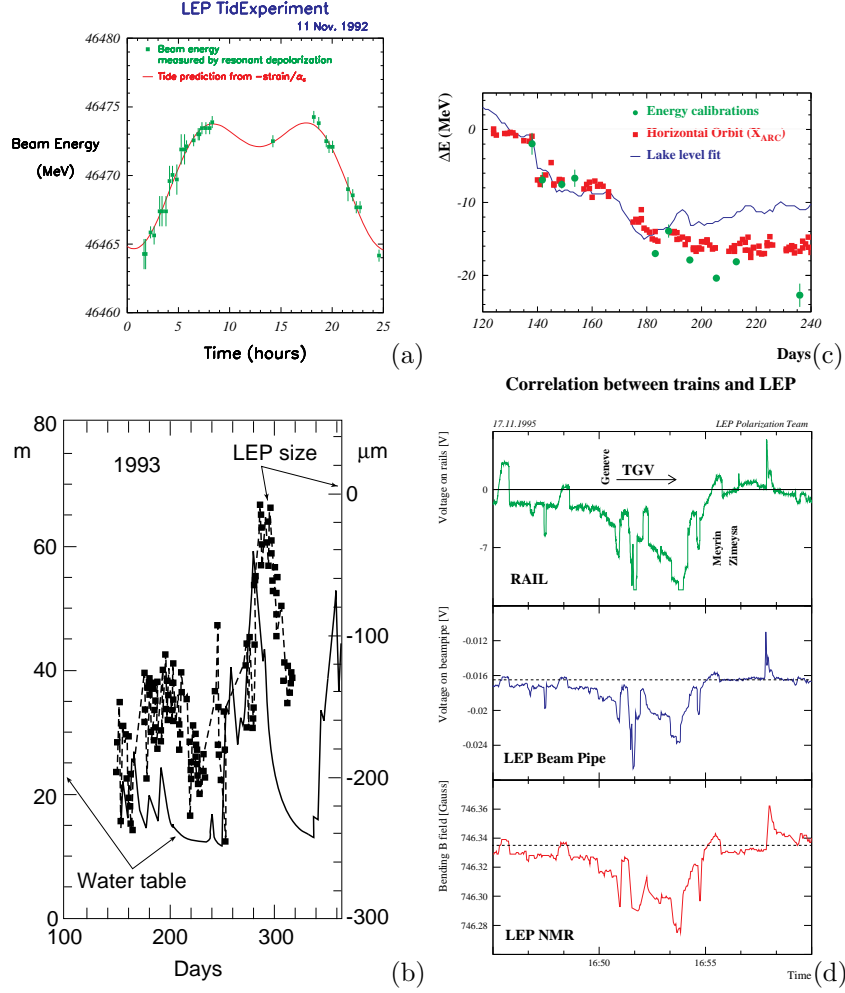


Figure 3: (a) Correlation of the LEP beam energy with tides. (b) Correlation of the LEP ring size with the height of the water table in the Jura mountains. (c) Correlation of the LEP beam energy with the orbit size and the water level in Lake Geneva. (d) Correlation between LEP beams and the passage of a TGV train.

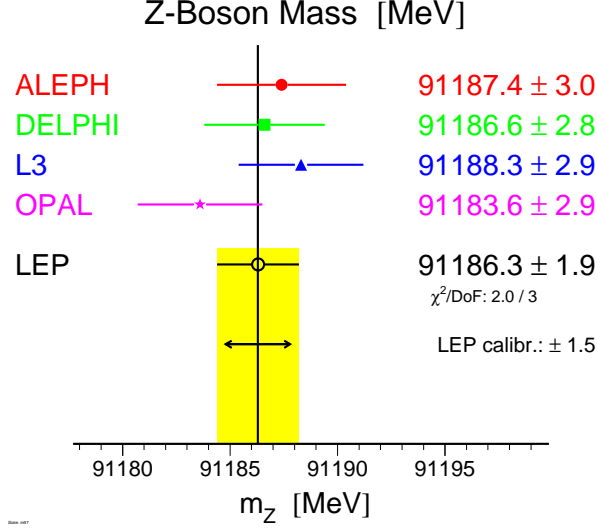


Figure 4: LEP measurements of m_Z , including the TGV effect.

1.2 Indirect Indications on m_H

At the one-loop level, using the mass-shell definition of $\sin^2 \theta_W$, Eq. (1.9) is modified to become

$$m_W^2 \sin^2 \theta_W = m_Z^2 \cos^2 \theta_W \sin^2 \theta_W = \frac{\pi \alpha}{\sqrt{2} G_\mu} (1 + \Delta r) \quad (1.10)$$

The one-loop quantum correction receives important contributions from the top quark¹²:

$$\Delta r \ni \frac{3 G_\mu}{8 \pi^2 \sqrt{2}} m_t^2 + \dots \quad (1.11)$$

for $m_t \gg m_b$. The divergence in (1.11) for large m_t reflects the fact that, without the top quark to complete the doublet started by the bottom quark, the gauge invariance of the Standard Model would be lost, and with it renormalizability and predictivity. Likewise, the Higgs boson plays an essential rôle in the spontaneous symmetry-breaking mechanism for generating particle masses, and the Standard Model would also be non-renormalizable in its absence. Thus we also expect a Higgs contribution to Δr that is divergent for large m_H . At

the one-loop level, this is only logarithmic¹³:

$$\Delta r \ni \frac{\sqrt{2}G_\mu}{16\pi^2} m_W^2 \left\{ \frac{11}{3} \ln \frac{m_H^2}{m_W^2} + \dots \right\} \quad (1.12)$$

for $m_H \gg m_W$, though numerically less important quadratically-divergent terms appear at higher-loop level.

Among other quantum-correction effects, we note that the ratio $\rho = 1 + \Delta\rho + \dots$ of low-energy neutral- and charged-current events in deep-inelastic ν scattering also depends quadratically on m_t , as does $Z^0 \rightarrow \bar{b}b$ decay⁶:

$$\frac{\Delta\Gamma_b}{\Gamma_b^0} \ni \frac{-20}{13} \frac{\alpha}{\pi} \left[\frac{m_t^2}{m_W^2} + \dots \right] \quad (1.13)$$

Moreover, much is known about the leading-order radiative corrections beyond one loop, for example the correction in (1.10): $1 + \Delta r \rightarrow 1/((1 - \Delta r))$, and¹⁴

$$\Delta\rho = \frac{3G_\mu}{8\pi^2\sqrt{2}} m_t^2 \left[1 - (2\pi^2 - 19) \frac{G_\mu m_t^2}{8\pi^2\sqrt{2}} + \dots \right] \quad (1.14)$$

These are also included in the codes used to analyze precision electroweak data¹⁵.

Such loop corrections also appear in all other electroweak observables. For example, Fig. 5 compiles the latest determinations³ of Γ_Z and shows how they compare with the Standard Model prediction as a function of m_t , m_H and the strong gauge coupling α_s . We see that the data have the potential to predict m_t , with some uncertainty due to m_H and α_s , that may be reduced by combining many different precision electroweak measurements. This feature is visible in Fig. 6, which compiles different determinations of the effective value of $\sin^2\theta_W$ on the Z^0 peak [which is closer to the $\overline{\text{MS}}$ definition than to the mass-shell definition used in (1.10)].

It was pointed out before LEP started operation that m_t could be predicted on the basis of precision electroweak data as soon as m_Z got measured precisely¹⁶, and predicting m_t has since become a major industry³. According to our latest analysis¹⁷, the best estimate of m_t , based on the data available since the summer of 1996 and treating m_H as a free parameter, is

$$m_t = 157_{-12}^{+16} \text{ GeV} \quad (1.15)$$

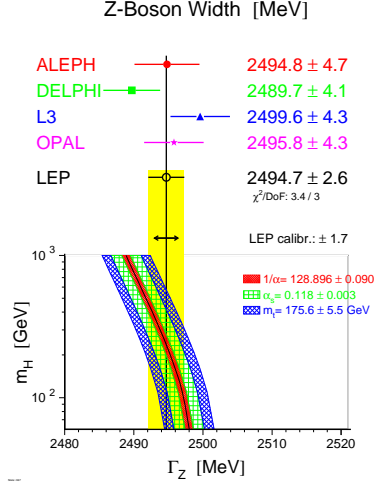


Figure 5: Measurements of the Z^0 width, including allowance for the TGV effect, compared with the Standard Model prediction as a function of α , α_s , m_t and m_H .

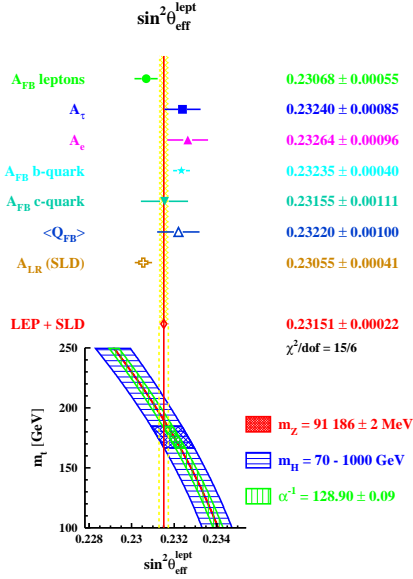


Figure 6: Different measurements of the effective $\sin^2 \theta_W$ at the Z peak.

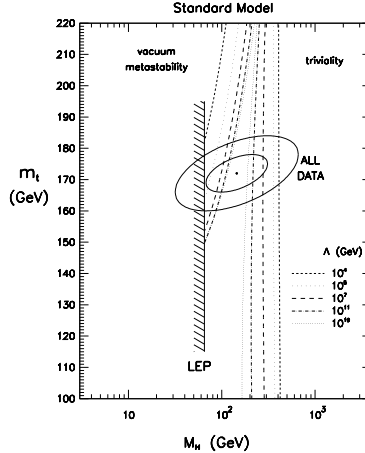


Figure 7: Global fit to the precision electroweak data and Fermilab measurements of m_t , compared with the LEP lower limit on m_H and the range expected if the Standard Model remains unmodified up to a scale Λ .

This is to be compared with the latest measurements by CDF and *D0* at Fermilab, which yield $m_t = 175 \pm 6$ GeV¹⁸. The good agreement between the indirect estimate and the direct measurement entitles one to combine them, as seen in Fig. 7, yielding $m_t = 172 \pm 6$ GeV.

Even in the absence of the direct measurement of m_t , the precision electroweak data alone provide some information about m_H , preferring a central value around 100 GeV^{17,3}. This estimate is sharpened if the direct measurement of m_t is included in the fit, yielding the estimate¹⁷

$$m_H = 145^{+164}_{-77} \text{ GeV} \left[\log\left(\frac{m_H}{\text{GeV}}\right) = 2.16 \pm 0.44 \right] \quad (1.16)$$

within the framework of the Standard Model.

The range (1.16) can be compared with the upper limit $m_H \lesssim 1$ TeV suggested by tree-level unitarity¹⁹, and the ranges allowed if the Standard Model couplings are required to remain finite if run up to some scale Λ using the renormalization group equations²⁰. For $\Lambda \sim_{GUT}$ or m_P , one requires $m_H \lesssim 200$ GeV, which is relaxed to $m_H \lesssim 650$ GeV if one takes $\Lambda = m_H$ itself, as in a lattice calculation²¹. There are also lower bounds on m_H which follow from

examining the behaviour of the Standard Model effective Higgs potential, and requiring that the standard electroweak vacuum be stable against transitions to any other state with $|H| \leq \Lambda$, or at least metastable with a lifetime longer than the age of the Universe²².

These bounds are compared in Fig. 7 with the range (1.16) favoured by the experimental measurements. We see that there is no indication of any breakdown of the Standard Model at any scale $\Lambda \lesssim m_P$. However, we nevertheless draw some encouragement for possible physics beyond the Standard Model, as discussed in the next section.

1.3 Motivations for Supersymmetry

The primary theoretical motivation for the appearance of supersymmetry²³ at accessible energies is to understand the origin of the large hierarchy of mass scales in physics²⁴: how and why is m_W so much smaller than m_P , the only candidate we have for a fundamental mass scale in physics? This question is made particularly acute by radiative corrections, which make such a hierarchy seem very unnatural. It is one thing to derive or postulate the existence of a very small bare mass parameter. It is another if radiative corrections to this bare quantity are very large, so that a small physical value can only be obtained at the price of an apparently conspiratorial cancellation between (almost) equal and opposite large bare and quantum contributions: the “fine-tuning” problem. This problem is not too acute for fermion masses m_f , whose one-loop correction has the form

$$\delta m_f = 0 \left(\frac{\alpha}{\pi} \right) m_f \ln \left(\frac{\Lambda}{m_f} \right) \quad (1.17)$$

where Λ is some cut-off representing an energy scale where the physics gets modified, which might be m_P at most. Because the divergence in (1.17) is only logarithmic, this correction is not much larger than the physical value of m_f , reflecting the fact that its smallness is safeguarded by chiral symmetry and poses no serious problem of naturalness or fine tuning.

This is, however, a problem for an elementary scalar boson, such as the Higgs boson of the Standard Model, whose mass must be within an order of magnitude of m_W : $m_W = 0 \left(\sqrt{\frac{\alpha}{\pi}} \right)^{0 \pm 1} m_H$. Each of the diagrams in Fig. 8a contributes a quadratically-divergent radiative correction

$$\delta m_H^2 \simeq g_{f,W,H}^2 \int^\Lambda \frac{d^4 k}{(2\pi)^4} \frac{1}{k^2} \simeq 0 \left(\frac{\alpha}{\pi} \right) \Lambda^2 \quad (1.18)$$

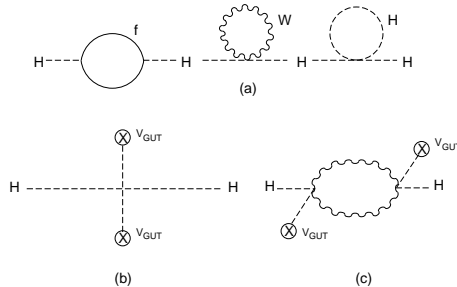


Figure 8: Potentially large contributions to m_H from (a) quadratic divergence in the Standard Model, (b) couplings to GUT Higgs bosons, and (c) logarithmic corrections to the latter.

which is many orders of magnitude larger than the physical value of m_H if we take $\Lambda \sim m_P$ or m_{GUT} ²⁴.

The remedy²⁴ offered by supersymmetry²³ is based on the fact that boson and fermion loops have opposite signs. Therefore, if one has equal numbers of bosons and fermions, and if their couplings are equal, the quadratically-divergent corrections will cancel:

$$\delta m_{W,H}^2 \simeq - \left(\frac{g_F^2}{4\pi} \right) (\Lambda^2 + m_F^2) + \left(\frac{g_B^2}{4\pi} \right) (\Lambda^2 + m_B^2) \simeq 0 \left(\frac{\alpha}{\pi} \right) (m_B^2 - m_F^2) \quad (1.19)$$

with a possible logarithmic factor, which is acceptably small ($\lesssim m_{W,H}^2$) if

$$|m_B^2 - m_F^2| \lesssim 1 \text{ GeV}^2 \quad (1.20)$$

Approximate supersymmetry also removes the threat of the GUT radiative corrections in Fig. 8c, though it does not by itself explain why the couplings in Fig. 8b should vanish. This naturalness argument provides the only theoretical argument why supersymmetry should appear at low energies, rather than (say) at m_P where it is apparently required for the consistency of string theory.

It should be emphasized, though, that this naturalness argument is qualitative, and rather a matter of taste. How much fine tuning of bare and one-loop masses is one prepared to tolerate: a factor of 2? 10? 100? Moreover, the Standard Model is mathematically consistent, in the sense that it is renormalizable and hence calculable, however much fine tuning there may be. The fine-tuning argument²⁴ is essentially one of physical intuition.

In the minimal supersymmetric extension of the Standard Model (MSSM)²⁵,

all the known particles are promoted to doublets (L, Q for lepton and quark doublets, E^c, U^c, D^c for charged lepton and quark singlets) with identical internal quantum numbers, but spins differing by half a unit. The supersymmetric part of the Lagrangian is determined by the gauge interactions, which are identical with those of the Standard Model, and by the superpotential:

$$W = \sum_{L, E^c} \lambda_L L E^c H_1 + \sum_{Q, U^c} \lambda_U Q U^c H_2 + \sum_{Q, D^c} \lambda_D Q D^c H_1 + \mu H_1 H_2 \quad (1.21)$$

The first three terms yield Yukawa couplings that give masses to the charged leptons, charge 2/3 and charge -1/3 quarks, respectively. Two Higgs doublets $H_{1,2}$ are needed to provide all the masses, in order to cancel triangle anomalies and for the superpotential to be holomorphic. In addition to the Yukawa interactions, the superpotential (1.21) provides, together with the gauge interactions, quartic self interactions of the scalar components of the supermultiplets, enabling predictions to be made for the masses of our quarries in this lecture, the physical Higgs bosons in the MSSM, as we shall discuss later.

In addition to the supersymmetric parts of the Lagrangian of the MSSM, there must be terms that break supersymmetry, providing in particular masses for the (as yet) unseen supersymmetric partners of the particles of the MSSM, such as the scalars: m_{0_i} and gauginos M_α . If these parameters are much larger than m_W , the latter becomes very sensitive to the choices of input parameters, and the fine-tuning problem returns. How large the (m_{0_i}, M_α) may be depends on the degree of fine tuning η that one is comfortable with^{26,27}:

$$\frac{\Delta m_W}{m_W} \leq \eta \frac{\Delta(\text{input})}{(\text{input})} \quad (1.22)$$

Figure 9 shows estimates of some sparticle masses obtained by requiring $\eta \leq 10$. We see that such an analysis favours relatively light sparticle masses: $m_{0_i}, M_\alpha \lesssim$ few hundred GeV, whether or not the scalar mass parameters m_{0_i} are assumed to be the same for all three generations of squarks²⁸. However, this is not a rigorous upper bound: in some sense, a more characteristic prediction of the MSSM is provided by the mass of the Higgs boson, as we discuss shortly.

To my mind, the precision electroweak data currently provide two tentative (s)experimental motivations for low-energy supersymmetry²⁹. One is the consistency of measurements of the gauge coupling strengths of the Standard Model with the hypothesis of supersymmetric grand unification. As seen in Fig. 10, when viewed on a scale from 0 to 1, the predictions of both supersymmetric and non-supersymmetric GUTs compare very well with the precision

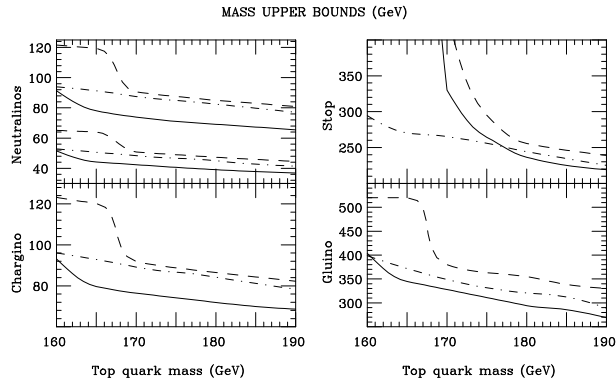


Figure 9: Upper bounds on sparticle masses, applying the condition (1.22) with $\eta = 10$, for universal scalar masses (dot-dashed lines) and non-universal masses (dashed lines). The solid lines are in the former case, neglecting loop corrections to Higgs boson masses.

electroweak measurements discussed earlier. Blowing the scale up by a factor 10 reveals a significant discrepancy with the non-supersymmetric GUT prediction, whereas the supersymmetric GUT prediction is satisfactory. Blowing the scale up by a further factor of 10 indicates that the sparticle masses cannot be exactly m_Z , but, to my mind, the electroweak data do not permit an interestingly precise indirect determination of the supersymmetric threshold. The second tentative experimental indication in favour of low-energy supersymmetry is provided by the apparent preference^{17,3} for a light Higgs boson manifested by the precision electroweak data which was discussed earlier, and is consistent with the prediction of the MSSM.

Since the MSSM contains two complex Higgs doublets, it contains eight real Higgs degrees of freedom, three of which become the longitudinal polarization states of the W^\pm and Z^0 , leaving five physical states. Three of these are neutral - two scalars h, H and one pseudoscalar A - and two are charged Higgs bosons H^\pm . At the tree level, all the MSSM Higgs masses and couplings are determined in terms of two parameters, which may be taken as the pseudoscalar mass m_A and the ratio of Higgs v.e.v.'s: $\tan \beta \equiv v_2/v_1$. For example, one has²⁵

$$m_{h,H}^2 = \frac{1}{2} [m_A^2 + m_Z^2] \mp \sqrt{(m_A^2 + m_Z^2)^2 - 4m_Z^2 m_A^2 \cos^2 2\beta} \quad (1.23)$$

from which one sees that $m_h < m_Z$ at the tree level. This lightness reflects the fact that the quartic Higgs self-coupling in the MSSM is relatively weak,

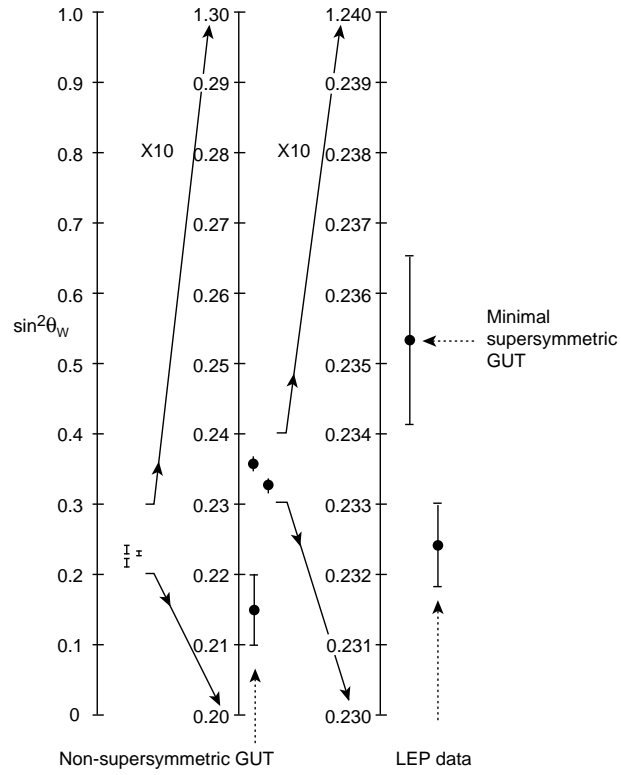


Figure 10: Measurements of $\sin^2 \theta_W$: note that the non-supersymmetric GUT prediction disagrees significantly with the data. The minimal supersymmetric GUT prediction assumes unrealistically that all sparticles have masses m_Z . Realistic spectra give predictions in agreement with the data.

since it originates from the electroweak D terms and is $0(g^2)$.

However, the upper bound on m_h is significantly relaxed by one-loop radiative corrections³⁰, which take the following form in the limit where the stop squark masses $m_{\tilde{t}_{1,2}}$ and $m_A \gg m_Z$:

$$\begin{aligned}
m_h^2 &= m_Z^2 \cos^2 2\beta + (\Delta m_h^2)_{ILL} + (\Delta m_h^2)_{mix} : \\
(\Delta m_h^2)_{ILL} &= \frac{3m_t^4}{4\pi^2 v^2} \ln \left(\frac{m_{\tilde{t}_1}^2 - m_{\tilde{t}_2}^2}{m_t^2} \right) \left[1 + 0 \left(\frac{m_W^2}{m_t^2} \right) \right] , \\
(\Delta m_h^2)_{mix} &= \frac{3m_t^4}{8\pi^2 v^2} \left[2h(m_{\tilde{t}_1}^2, m_{\tilde{t}_2}^2) + \tilde{A}_t^2 f(m_{\tilde{t}_1}^2, m_{\tilde{t}_2}^2) \right] \\
&\quad \left[1 + 0 \left(\frac{m_W^2}{m_t^2} \right) \right]
\end{aligned} \tag{1.24}$$

where $\tilde{A}_t \equiv A_t - \mu \cot \beta$ and

$$h(a, b) \equiv \frac{1}{a - b}, \quad f(a, b) \equiv \frac{1}{(a - b)^2} \left[2 - \left(\frac{a + b}{a - b} \right) \ln \left(\frac{a}{b} \right) \right] \tag{1.25}$$

One-loop corrections to Higgs coupling vertices are also known, as are the leading two-loop corrections to the Higgs mass, for which accurate renormalization-group-improved formulae are known³¹.

As seen in Fig. 11, the net effect of the radiative corrections is to increase the maximal h mass to about 150 GeV. The allowed range for different $\tan \beta$ is compares well with the range preferred by the precision electroweak data for different m_t shown in Fig. 7. These correspond to a probability of 32 % that the true values of m_t and the Higgs mass lie in the range allowed by the MSSM, compared to 27 % for the range allowed by the Standard Model if no new physics intervenes below the Planck scale¹⁷. Supersymmetry is certainly consistent with the data, though we cannot yet exclude its absence!

1.4 Higgs Search at LEP 2

The dominant mechanism for Higgs production at LEP 2 in the Standard Model is $e^+e^- \rightarrow Z^0 + H$ ², whose tree-level cross section is

$$\sigma_{ZH} = \frac{G_F^2 m_Z^4}{96\pi s} (v_e^2 + a_e^2) \lambda^{1/2} \frac{\lambda + 12m_Z^2/s}{(1 - m_Z^2/s)^2} \tag{1.26}$$

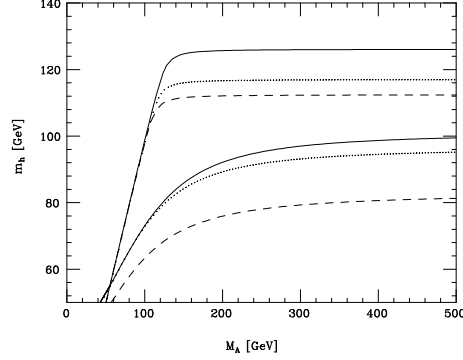


Figure 11: The radiatively-corrected mass of the lightest MSSM Higgs boson mass m_h as a function of m_A , for $\tan \beta = 1.6$ (lower curves) and 15 (upper curves), and maximal mixing (solid lines), minimal mixing (dashed lines), and intermediate mixing (dotted lines), assuming $m_t = 175$ GeV and $m_{\tilde{q}} = 1$ TeV.

where $a_e = -1$ and $v_e = -1 + 4 \sin^2 \theta_W$ are the $Z^0 e^+ e^-$ couplings in the Standard Model, and $\lambda = (1 - m_H^2 s - m_Z^2/s)^2 - 4(m_H^2 m_Z^2/s^2)$ is the conventional two-body phase-space factor. The proper electroweak radiative corrections to (1.26) are small¹: $\delta\sigma/\sigma \lesssim 1.5\%$. More important are initial-state radiative (ISR) corrections, which in leading order give

$$\langle \sigma \rangle = \int_{x_H}^1 dx G(x) \sigma(xs) \quad (1.27)$$

where $x_H \equiv m_H^2/s$ and $G(x)$ is a “radiator function”, which is known to $O(\alpha^2)$ ¹. In addition, one must allow for off-shell Z^0 production by incorporating finite-width effects. To understand the full reach of LEP 2 for the Higgs search, one must also take into account the reaction $e^+ e^- \rightarrow \bar{\nu}_e H \nu_e$, due to $W^+ W^-$ fusion³². All these effects are included in Fig. 12.

Since the Higgs couplings to other particles are proportional to their masses, the dominant Higgs decays are those into the heaviest available particles (see the first paper in²), notably $H \rightarrow \bar{b}b$ ¹:

$$\Gamma(H \rightarrow \bar{b}b) \simeq \frac{3G_F}{4\sqrt{2}\pi} m_b^2 (m_H) m_H \left[1 + 5.67 \left(\frac{\alpha_s}{\pi} \right) + \dots \right] \quad (1.28)$$

to be compared with $H \rightarrow \tau^+ \tau^-$:

$$\Gamma(H \rightarrow \tau^+ \tau^-) \simeq \frac{G_F}{4\sqrt{2}\pi} m_\tau^2 m_H \quad (1.29)$$

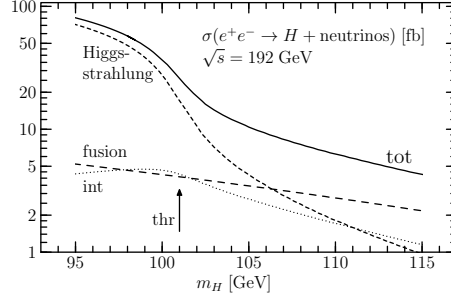


Figure 12: Cross section for Higgs boson production at LEP 2, including $e^+e^- \rightarrow (Z \rightarrow \bar{\nu}\nu) + H$ and $e^+e^- \rightarrow \nu_e\bar{\nu}_e + H$.

as well as $H \rightarrow \bar{c}c$ which is given by (1.28) with $m_b \rightarrow m_c$, and $H \rightarrow gg$ which is dominated by top loops:

$$\Gamma(H \rightarrow gg) \simeq \frac{G_F \alpha_s^2(m_H)}{36\sqrt{2}\pi^3} m_H^3 \quad (1.30)$$

The decays $H \rightarrow \gamma\gamma$, W^+W^- and Z^0Z^0 , are not important at LEP 2, though they are important for LHC Higgs searches³³. The total Higgs decay width Γ_H is less than 3 MeV for $m_H < 100$ GeV.

Each individual LEP experiment has one or two candidate events for Standard Model Higgs production, but these do not coincide in mass. Individual experiments limit $m_H \gtrsim 70$ GeV³⁴, and the combined LEP limit so far is estimated to be $m_H \gtrsim 75$ to 77 GeV. Eventually, experiments at LEP 2 should be sensitive to $m_H \lesssim E_{cm} - m_Z$ – few GeV, or $m_H \lesssim 95(100)$ GeV if the maximum E_{cm} reaches 192(200) GeV.

In the context of the MSSM, there are two interesting Higgs production processes: $e^+e^- \rightarrow Z^0h$ and $e^+e^- \rightarrow Ah$. The former has a tree-level cross section smaller than that for $e^+e^- \rightarrow Z^0H$ in the Standard Model by a factor $\sin^2(\beta - \alpha)$ where α is a mixing angle in the Higgs sector¹. Fortunately, $\sigma(e^+e^- \rightarrow Ah) \propto \cos^2(\beta - \alpha)$, so that there is some complementarity between these two processes, unless m_A is large. The dominant supersymmetric Higgs decay modes are likely to be similar to those in the Standard Model, though there is a nightmare possibility that invisible $hA \rightarrow \chi\chi$ decays might dominate! Ignoring, for the moment, this possibility which is in any case disfavoured by the lower limit on m_χ discussed in Lecture 3, the unsuccessful searches so far for $e^+e^- \rightarrow Z^0h$ and Ah indicate that $m_h \gtrsim 63$ GeV³⁵, whatever the value of

$\tan \beta$. Because of the radiative correction (1.24), (1.25), there is no guarantee that LEP 2 will find the lightest supersymmetric Higgs boson. Fortunately, it seems that the LHC will be able to complete the coverage of MSSM parameter space.

2 *W* Physics

2.1 *W* Mass

The world average of direct measurements from experiments other than those at LEP yields³

$$m_W = 80.37 \pm 0.08 \text{ GeV} \quad (2.1)$$

and is dominated by measurements at the Fermilab $\bar{p}p$ collider⁸. This can be compared with the theoretical prediction that one makes within the Standard Model, using a global fit to the precision electroweak data³:

$$m_W = 80.323 \pm 0.042 \text{ GeV} \quad (2.2)$$

A large fraction of this error: (+13, -24) MeV is associated with uncertainty in the Higgs mass: $60 \text{ GeV} < m_H < 1 \text{ TeV}$ as seen in Fig. 13¹. This arises principally via the one-loop radiative correction Δr to m_W :

$$G_\mu = \frac{\alpha\pi}{\sqrt{2}} \frac{m_W^2}{(1 - m_W^2/m_t^2)} \frac{1}{1 - \Delta r} \quad (2.3)$$

whose leading m_H -dependence was given was Eq. (1.12).

A more precise direct measurement of m_W would help constrain m_H within the Standard Model, as well as constrain possible extensions such as supersymmetry. As an example of the possible impact on m_H , Table 2 lists the errors in m_H that would result from measurements of m_W with errors of 25 and 50 MeV, assuming that m_t is measured to be $180 \pm 5 \text{ MeV}$ ¹. We see that a direct measurement of m_W with an error between 25 and 50 MeV, which seems possible at LEP 2, would have significant impact on the prediction of m_H within the Standard Model.

Two methods of measuring m_W at LEP 2 appear to be the most promising. One is from the threshold cross section for $e^+e^- \rightarrow W^+W^-$, which could yield¹

$$\Delta m_W \geq 91 \text{ GeV} \sqrt{\frac{100 \text{ pb}^{-1}}{\mathcal{L}}} \quad (2.4)$$

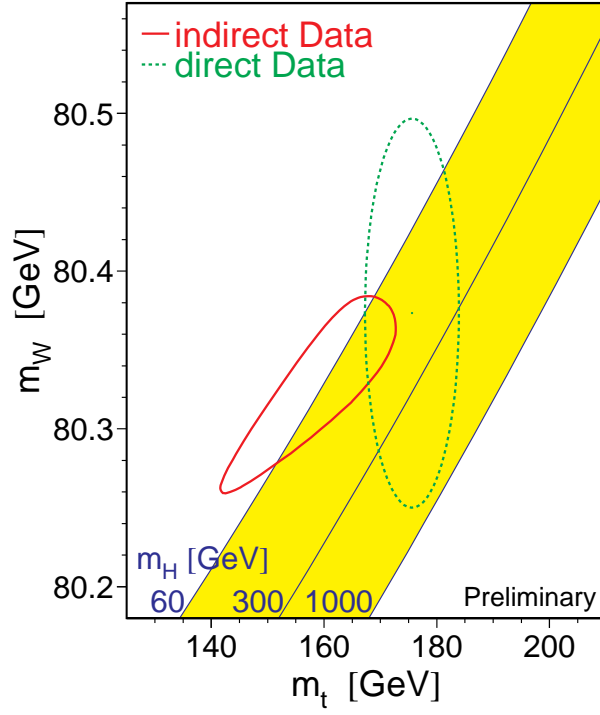


Figure 13: Indirect predictions of m_t and m_W (solid line) based on precision electroweak data from LEP and elsewhere, compared with the present direct measurements (dashed line) and calculations for different values of m_H .

Table 2: Errors in M_H for assumed errors in m_W

Nominal Value of m_H	Δm_W	
	25 MeV	50 MeV
100	(+ 86, - 54)	(+140, -72)
300	(+196, -126)	(+323, -168)

where \mathcal{L} is the accumulated luminosity. The inequality (2.4) is saturated at $E_{CM} = 161$ GeV under the idealized assumptions that W^+W^- events are selected with 100 % efficiency and no background. Theoretical issues arising in the calculation of $\sigma(e^+e^- \rightarrow W^+W^-)$ are discussed in Section 2.2.

Alternatively, one may measure m_W by the direct reconstruction of W^\pm decays, which should yield¹

$$\Delta m_W \geq \frac{\Gamma_W}{\sqrt{N}} \simeq 50 \text{ MeV} \sqrt{\frac{100 pb^{-1}}{\mathcal{L}}} \quad (2.5)$$

This estimate is valid at any centre-of-mass energy above about 170 GeV, again under the idealized assumptions of 100 % efficiency, no background and perfect detector resolution. In practice, the classes of W^+W^- events that can be used for such direct reconstruction are $(W^\pm \rightarrow \bar{q}q)$ ($W^\mp \rightarrow \ell\nu$) and $(W^+ \rightarrow \bar{q}q)$ ($W^- \rightarrow \bar{q}q$). In the latter case, questions arise whether the W^\pm hadronize independently, and whether any interference or collective effects such as colour reconnection³⁶ and Bose-Einstein correlations³⁷ have a significant impact on the error (2.5) with which m_W may be measured. This problem will be discussed in Section 2.3 with particular emphasis on our analysis^{38,39,40} of the space-time development of $e^+e^- \rightarrow W^+W^- \rightarrow$ hadrons events.

Finally, it should be noted that one could in principle measure m_W using the end-point energy of the $W^\pm \rightarrow \ell^\pm \nu$ spectrum:

$$\Delta m_W = \frac{\sqrt{S - m_W^2}}{m_W} \Delta E_{L^\pm} \quad (2.6)$$

Unfortunately, the end point is so smeared by finite-width and ISR effects, and so limited in statistics, that it does not appear to be a competitive way to determine m_W ¹.

2.2 Cross-Section for $e^+e^- \rightarrow W^+W^-$

Since the W^\pm are unstable, the W^+W^- final state must be considered in conjunction with other mechanisms for producing the same four-fermion final states, which are in principle indistinguishable¹. Indeed, any separation

$$\sigma_{4f} = \sigma_{W^+W^-} + \sigma_{bkgrd} \quad (2.7)$$

is not even gauge invariant! The W^+W^- contribution in (2.7) can be further decomposed in the form:

$$\sigma_{W^+W^-} = \sigma_{W^+W^-}^0 (1 + \delta_{ew} + \delta_{QCD}) + \dots \quad (2.8)$$

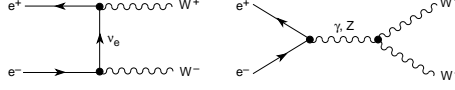


Figure 14: Lowest-order CC03 diagrams for $e^+e^- \rightarrow W^+W^-$.

where $\sigma_{W^+W^-}^0$ is the tree-level Born cross-section for producing off-shell W^\pm via the three “classic” ν -, γ - and Z^0 -exchange “CC03” diagrams shown in Fig. 14, $\delta_{ew,QCD}$ represent one-loop electroweak and QCD corrections, respectively and the dots in (2.8) represent higher-order corrections. The off-shell tree-level cross section $\sigma_{W^+W^-}^0$ may in turn be written as

$$\sigma_{W^+W^-}^0(s) = \int_0^s ds_1 \int_0^{(\sqrt{s}-\sqrt{s_1})^2} ds_2 \rho(s_1) \rho(s_2) \sigma^0(s, s_1, s_2) \quad (2.9)$$

where

$$\rho(s) = \frac{1}{\pi} \frac{\Gamma_W}{m_W} \frac{s}{(s - W_W^2)^2 + s^2 \Gamma_m^2 / m_W^2} \quad (2.10)$$

is a relativistic Breit-Wigner spectral function with a mass-dependent width $\Gamma_W(s) = s\Gamma_W/m_W^2$.

The tree-level cross-section $\sigma^0(s, s_1, s_2)$ in (2.9) may be obtained from the Born matrix elements:

$$\mathcal{M}_B = \frac{e^2}{2s_W^2} \frac{1}{t} \mathcal{M}_1 \delta_L + e^2 \left(\frac{1}{s} - \cot \theta_W g_{eeZ} \frac{1}{s - m_Z^2} \right) 2(\mathcal{M}_B - \mathcal{M}_Z) \quad (2.11)$$

where $\delta_L = 1, 0$ for $e_{L,R}$ and $g_{eeZ} = \tan \theta_W - \delta_L \frac{1}{2 \sin \theta_W \cos \theta_W}$. Close to threshold, one has $\mathcal{M}_1 \sim 1$ and $\mathcal{M}_{2,3} \sim \beta$, so the cross-section is dominated by t -channel ν exchange, which yields an angular distribution

$$\frac{d\sigma}{d\theta} = \frac{\alpha^2}{s} \frac{1}{4 \sin^4 \theta_W} \beta \left[1 + 4\beta \cos \theta \frac{3 \cos^2 \theta_W - 1}{4 \cos^2 \theta_W - 1} + 0(\beta^2) \right] \quad (2.12)$$

and a cross-section

$$\sigma = \frac{\pi \alpha^2}{s} \cdot \frac{1}{4 \sin^4 \theta_W} \cdot 4\beta + 0(\beta^3) \quad (2.13)$$

close to threshold. This yields a sharp threshold rise, but does mean that the cross-section close to threshold is not very sensitive to the triple-gauge couplings to be discussed in Section 2.4.

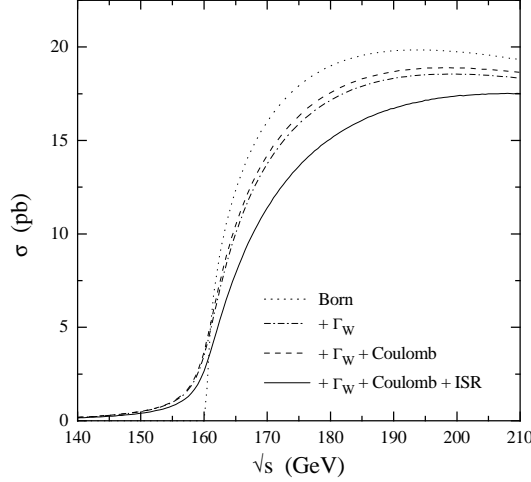


Figure 15: Threshold cross section for $e^+e^- \rightarrow W^+W^-$, including finite-width effects, Coulomb corrections and Initial-State Radiation (ISR).

The one-loop electroweak corrections δ_{ew} in (2.8) are completely known for on-shell W^\pm , but only the leading contributions $\sim \ln(s/m_e^2)$, $\sqrt{(m_W/\Gamma_W)}$, m_t^2/m_W^2 , \dots are fully known for off-shell W^\pm ¹. Comparing the “CC03” cross-section with calculations of all the 11 diagrams contributing to $e^+e^- \rightarrow \mu^- \bar{\nu} u \bar{d}$ suggests that the residual theoretical error in the cross-section $\delta\sigma/\sigma \lesssim 2\%$. As seen in Fig. 15, important rôles in reaching this precision are played by ISR corrections, for which the formalism in (1.27) can be used, and Coulomb corrections near threshold. These blow up for stable on-shell particles: $\delta\sigma/\sigma \sim \alpha\pi/v_0 : v_0 = \sqrt{1 - (4m_W^2/s)}$, but are cut off in this case by the finite width of the W^\pm : $\alpha\pi/v_0 \rightarrow \alpha\pi\sqrt{(m_W/\Gamma_W)}$: the W^\pm decay before they can be bound!⁴¹ As seen in Fig. 15, the Coulomb correction is about 6 % in the threshold region, corresponding to an error of about 100 MeV in m_W if it were not included.

The statistical error in measuring the W^+W^- cross-section is

$$\Delta\sigma_{W^+W^-} = \frac{\sigma_{W^+W^-}}{\sqrt{N_{W^+W^-}}} = \frac{\sqrt{\sigma_{W^+W^-}}}{\sqrt{\epsilon_{W^+W^-}\mathcal{L}}} \quad (2.14)$$

where $N_{W^+W^-}$ is the number of events recorded, which depends on the efficiency $\epsilon_{W^+W^-}$ as well as the accumulated luminosity \mathcal{L} . The corresponding error in m_W is¹

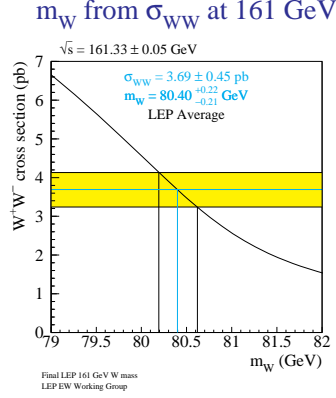


Figure 16: Measurement of m_W from the threshold cross-section for $e^+e^- \rightarrow W^+W^-$ at LEP.

$$\Delta m_W = \sqrt{\sigma_{W^+W^-}} \left| \frac{dm_W}{d\sigma_{W^+W^-}} \right| \frac{1}{\sqrt{\epsilon_{W^+W^-} \mathcal{L}}} \quad (2.15)$$

The first two factors in (2.15) govern the sensitivity of the threshold cross-section method of measuring m_W , and are minimized around $0.91 \text{ GeV}/\sqrt{pb}$ when $E_{cm} \simeq 2m_W + 0.05 \text{ GeV}$. On the basis of this and the previous world average determination of m_W (not to mention the availability of superconducting radio-frequency cavities), a centre-of-mass energy $E_{cm} = 161.33 \pm 0.05 \text{ GeV}$ was chosen for the threshold LEP 2W run in the summer of 1996. The accumulated luminosities were about 10 pb^{-1} per experiment, for which systematic errors associated with σ_{bkgd} , $\epsilon_{W^+W^-}$, etc., were relatively unimportant. The resulting measurement of $\sigma_{W^+W^-}$ provided the measurement³

$$m_W = 80.40^{+0.22}_{-0.21} \text{ GeV} \quad (2.16)$$

as seen in Fig. 16.

2.3 Kinematic Reconstruction of $e^+e^- \rightarrow W^+W^-$

As already mentioned, this is the way to measure m_W at higher centre-of-mass $E_{cm} \geq 170 \text{ GeV}$. The wholly leptonic final states ($W^+ \rightarrow \ell^+\nu$) ($W^- \rightarrow \ell^-\bar{\nu}$) are not useful in this respect, since they have two missing neutrinos and a small branching ratio of about 10 %. The semileptonic decays ($W^\pm \rightarrow \ell^\pm\nu$) ($W^\mp \rightarrow$

Table 3:

Source	$W^+W^- \rightarrow q\bar{q}q\bar{q}$	$W^+W^- \rightarrow q\bar{q}\ell\nu$
E_{beam}	12	12
ISR	10	10
fragmentation	16	16
backgrounds	12	6
calibration	10	10
MC statistics	10	10
mass fit	10	10
jet assignment	5	-
interconnection	?	-
Total	31	29

$\bar{q}q$) are much more useful, since they have a larger branching ratio $\sim 45\%$, it is possible to select efficiently a small-background sample, and the final states can be reconstructed in a constrained fit¹. The wholly hadronic decays ($W^+ \rightarrow \bar{q}q$) ($W^- \rightarrow \bar{q}q$) have a similar branching ratio and one can in principle make a more highly-constrained fit, but the background problems are more severe, and there are the problems of colour reconnection³⁶ (or cross-talk, or exogamy⁴⁰) between the hadronic showers of the W^\pm pair and of distortions induced by Bose-Einstein correlation effects³⁷ to be discussed shortly.

Figure 17 compares the expected signals and backgrounds in the semileptonic and purely hadronic final states, and Table 3 compiles the systematic and statistical errors in the corresponding determinations of m_W ¹, setting aside possible colour reconnection and Bose-Einstein effects. Most estimates have suggested that these may be ≤ 50 MeV¹, but one would like to be able to cross-check these estimates³⁹. This seems to require a deeper understanding of the space-time development of hadronic showers in e^+e^- annihilation³⁸, which we now discuss.

Consider first the process $e^+e^- \rightarrow Z^0 \rightarrow \bar{q}q \rightarrow \text{hadrons}$ ³⁸. The initial Z^0 decay is to a pair of “hot” off-shell partons, which can be regarded as creating a localized “hot spot” of the quark-gluon “parton phase” of QCD, surrounded by the usual “cold” hadronic vacuum with condensates $\langle 0|\bar{q}q|0 \rangle > 0$, $\langle 0|G_{\mu\nu}^a G_a^{\mu\nu}|0 \rangle \neq 0$ “frozen” in, as seen in Fig. 18. In the subsequent perturbative parton shower development, the “hotter” highly virtual partons decay into “cooler” partons closer to mass shell: the “hot spot” expands and “cools”.

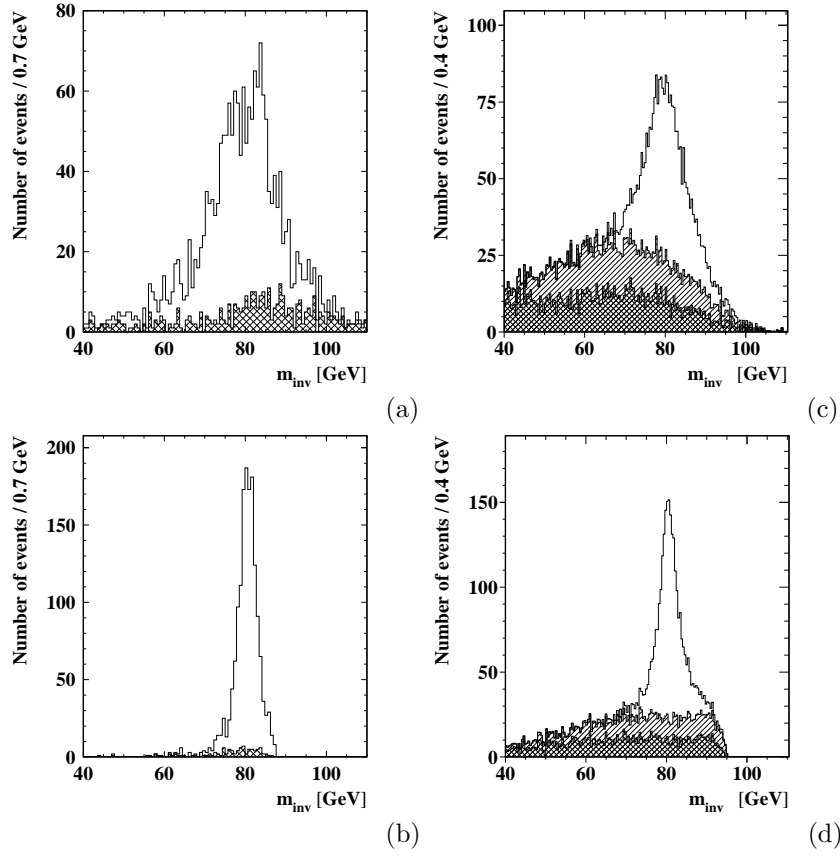


Figure 17: Reconstructed hadronic W mass distributions for (a,b) $W^+W^- \rightarrow \bar{q}q\ell\nu$ events and (c,d) $W^+W^- \rightarrow (\bar{q}q)(\bar{q}q)$ events, both before (a,c) and after (b,d) background event deselection.

Since confinement forbids the isolation of any parton, whenever a parton separates to $\gtrsim 1$ fm from its nearest-neighbour partons, it should be confined and participate in hadronization. This takes place at different times in different regions of the parton shower, and the process continues until all partons “cool”, separate and hadronize.

The initial stages of this parton shower development can be modelled using a conventional perturbative QCD Monte Carlo in which spatial locations are also followed³⁸. The lifetime t_p of a parton obeys $\langle t_p(x, k^2) \rangle = \gamma\tau \simeq E/k^2 = xQ/2k^2$, where τ is its proper lifetime, k^2 is virtuality, and x its beam energy fraction. Its subsequent chain of decays into “cooler” partons lasts a time after n steps:

$$t^{(n)} : \langle t^{(n)} \rangle = \sum_{i=1}^n \langle t_i \rangle = \frac{Q}{2} \sum_{i=1}^n \frac{x_i}{k_i^2} . \quad (2.17)$$

For soft partons in a perturbative QCD cascade, one finds the total time lapse

$$\langle t(x, k^2) \rangle \sim a \frac{xQ}{2k^2} \exp(-b\sqrt{\ln(1/x)}) \quad (2.18)$$

corresponding to the familiar “inside-outside cascade”.

This behaviour can be modelled in a perturbative QCD Monte Carlo programme in which the quantum transport equations are correctly implemented⁴², including the time development. This is followed in short-time steps, with branching (and in principle recombination) processes occurring stochastically at rates with the means (2.17). At each time step, the spatial locations of all the partons are recorded and the invariant separation of parton pairs measured. Whenever any parton becomes separated from its nearest neighbour by an amount $\Delta r \simeq L_c$, where L_c is a critical length parameter, the parton hadronizes by coalescence with this nearest neighbour, possibly with parton emission to preserve colour and global quantum numbers. Figure 19 shows the time developments of parton and hadron numbers and distributions in three implementations of this non-perturbative model which treat hadronization with increasing attention to the colour degrees of freedom^{38,39}. They share the feature that hadronization occurs gradually over a period $\frac{1}{2}fm/c \lesssim t \lesssim 10fm/c$.

More specifically, our model for parton-hadron conversion is based on an effective Lagrangian description of the low-energy “cool” hadron phase, which manifests the chiral symmetry of almost massless pions and kaons:

$$\mathcal{L}_{QCD} \rightarrow \mathcal{L}_{eff}(\pi, K, \dots) . \quad (2.19)$$

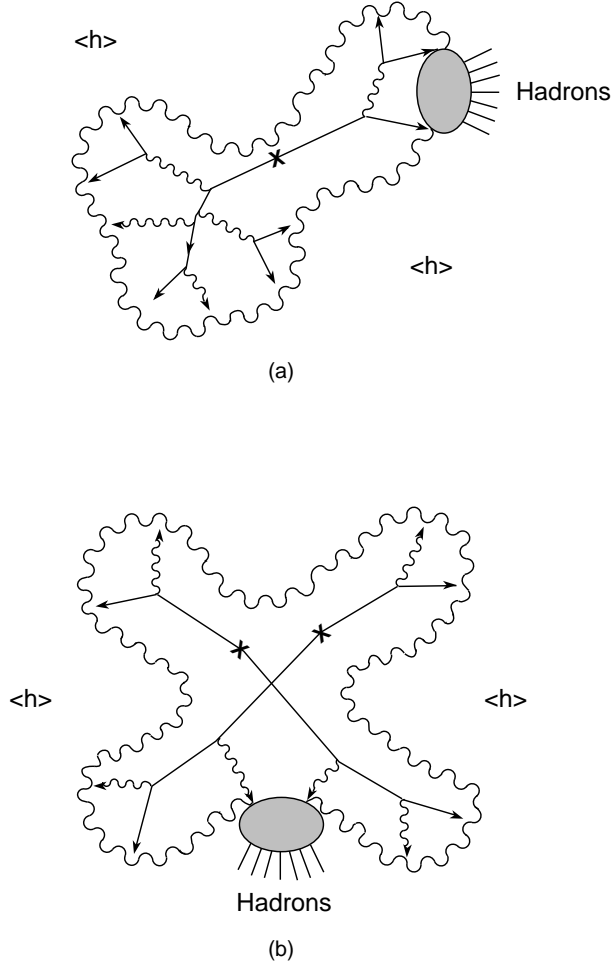


Figure 18: Parton shower development and hadronization in (a) Z^0 decay and (b) W^+W^- decay is viewed as a “hot” spot expanding from the decay vertices, marked with crosses, into the conventional “cold” hadronic vacuum $\langle h \rangle$, with clusters of hadrons forming whenever a parton gets separated from its nearest neighbour by about 1 fm.

TIME EVOLUTION OF PARTICLES AND 4-MOMENTUM

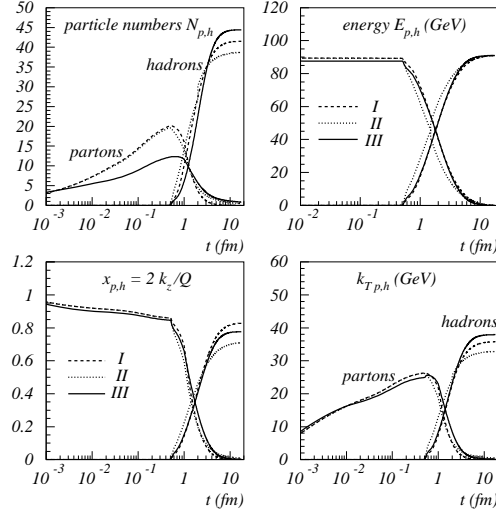


Figure 19: Time evolution of parton and hadron distributions in a space-time model for parton shower development and hadronization, using three different scenarios (I, II, III) for cluster formation.

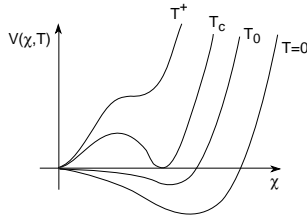


Figure 20: Sketch of the temperature dependence of the effective QCD potential, as a function of a hadronic order parameter χ related to condensates $\langle h \rangle$. One expects similar behaviour for a finite-size QCD system, with $T \rightarrow 1/L$.

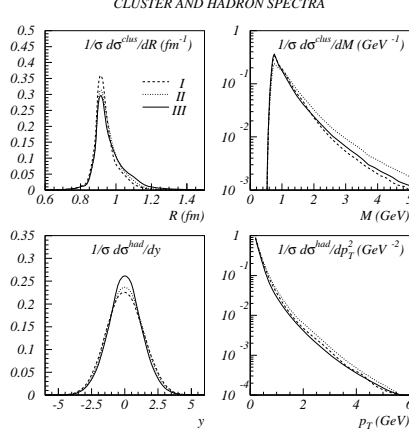


Figure 21: Cluster and hadron distributions in the same model as used in Fig. 19.

Within this model, the quark-hadron phase transition at finite temperature T and negligible chemical potential can be described using conventional field-theoretical techniques⁴³. One finds a critical temperature $T_c = O(\Lambda_{QCD})$ at which the conventional perturbative QCD vacuum and the “cold” non-perturbative QCD vacuum have equivalent free energies. If one quantizes the effective theory (2.19) in a finite volume instead of at finite temperature, one finds a corresponding transition at a critical size $L_c = O(1/T_c)$ ³⁸. The transition is expected to be a tunnelling phenomenon analogous to that through the finite-temperature barrier in Fig. 20. The conversion process is actually stochastic with a probability that is peaked at sizes $R \gtrsim L_c$. Figure 21 shows how the sizes of hadronic clusters in three different colour implementations of this approach for $e^+e^- \rightarrow Z^0 \rightarrow \text{hadrons}$, together with some resulting hadron distributions³⁸. The time evolutions of parton and hadron spectra are shown in Fig. 19. As seen in Fig. 22, this model reproduces the expected inside-outside cascade picture. x

After this introduction, we are now ready to apply this approach to the process $e^+e^- \rightarrow W^+W^- \rightarrow \text{hadrons}$ ^{39,40}.

The first point to notice in this case is that the $W^+W^- \rightarrow (\bar{q}q)(\bar{q}q)$ decays occur almost on top of each other, after times $t^\pm :< t^* >= \gamma/\Gamma_W$, separated by a distance $|r^+ - r^-| :< r^\pm >= (\gamma/\Gamma_W) (1, \beta^\pm)$. Using the Standard Model value for Γ_W , one finds a typical separation $|r^+ - r^-| \lesssim 0.1$ fm. Hence,

INSIDE-OUTSIDE HADRON FORMATION

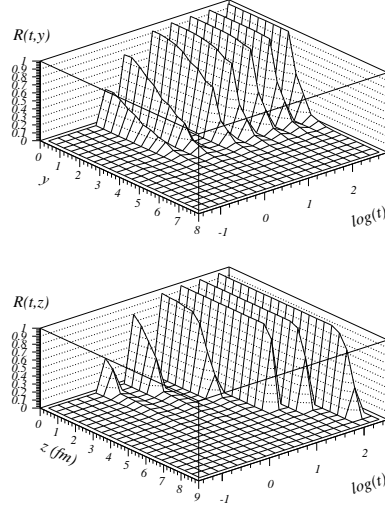


Figure 22: Space-time development of the inside-outside cascade in the same model as used in Figs. 19 and 21.

the W^+W^- decays form a single “hot spot”, not two, as seen in Fig. 18, and are followed by parton showering that is approximately simultaneous and coincidental. *A priori*, a parton from one W does not “know” that it should hadronize with another parton from the same shower in an “endogamous” union, and may prefer to hadronize with a parton from the other W in an “exogamous” union. In our approach, each parton chooses its hadronization partner purely on the basis of its propinquity, not its shower ancestry. This is a non-perturbative extension of the observation already made some time ago in perturbation theory that the W^\pm parton showers are not independent³⁶. However, perturbative colour reconnection effects are known to be very small: $\mathcal{O}(\alpha_s/\pi)^2/N_c$.

The fact that the $W^\pm \rightarrow \bar{q}q$ do not hadronize independently means that the final-state hadron distributions differ, in general, from hypothetical “infinitely-separated” W^\pm pairs. Indeed, the question which hadron comes from which W^\pm does not even have a well-defined answer. In particular, these differences in the final-state hadron distributions can be expected to have an effect on m_W which is $\mathcal{O}(\Lambda_{QCD})$. We have studied this possible effect in different variants

of our parton-hadron conversion model, using scenarios which differ in their treatment of the colour book keeping. We found mass shifts³⁹

$$\delta m_W|_{\text{real-hypo}} = (-13, +6, +280) \text{ MeV} \quad (2.20)$$

between the masses extracted using standard jet algorithms in the realistic case of overlapping W^\pm and a hypothetical situation with W^\pm decays separately widely in space, which could exceed the statistical and systematic errors mentioned previously.

In view of the potential gravity of this colour-reconnection effect, it is desirable to identify possible observational signatures that could give advance warning of such a phenomenon⁴⁰. One possibility is that the difference in hadronization could show up directly as a change in the total hadronic multiplicity:

$$\langle n \rangle_{W^+W^- \rightarrow \bar{q}q\bar{q}q} \neq 2 \langle n \rangle_{(W^\pm \rightarrow \bar{q}q)} \quad (2.21)$$

As shown in Fig. 23, this effect could be substantial, possibly as large as 10 %. Such a large effect would also show up in the mean transverse momenta, as also shown in Fig. 23, because the total transverse energies of the initial-state $\bar{q}q$ jets have to be shared between fewer hadrons. Differences may also show up in the longitudinal momentum or rapidity distributions, as shown in Fig. 24. It is understandable that the effect should be larger for slower particles, which are more confused about their origins, since the slower partons overlap more than the faster ones. The effect extends also to faster partons if the W^\pm decay into $\bar{q}q$ dijets that are almost antiparallel, as seen in Fig. 25. The initial studies of W^\pm final states with data taken during 1996 do not reveal any gross features of this type⁴⁴, but the statistics are quite limited. It is to be hoped that the greater statistics to be gathered in 1997 will permit a more detailed study of this question.

To conclude this section, Fig. 26 shows a compilation³ of present measurements of m_W from $\bar{p}p$ colliders (dominated by FNAL⁸) and from LEP2, including both the threshold and reconstruction methods, and assuming in the latter case that the hadronic “exogamy” and Bose-Einstein effects are negligible at the present level of statistics. Also shown for comparison is the Standard Model prediction, based on precision electroweak measurements from LEP and the SLC.

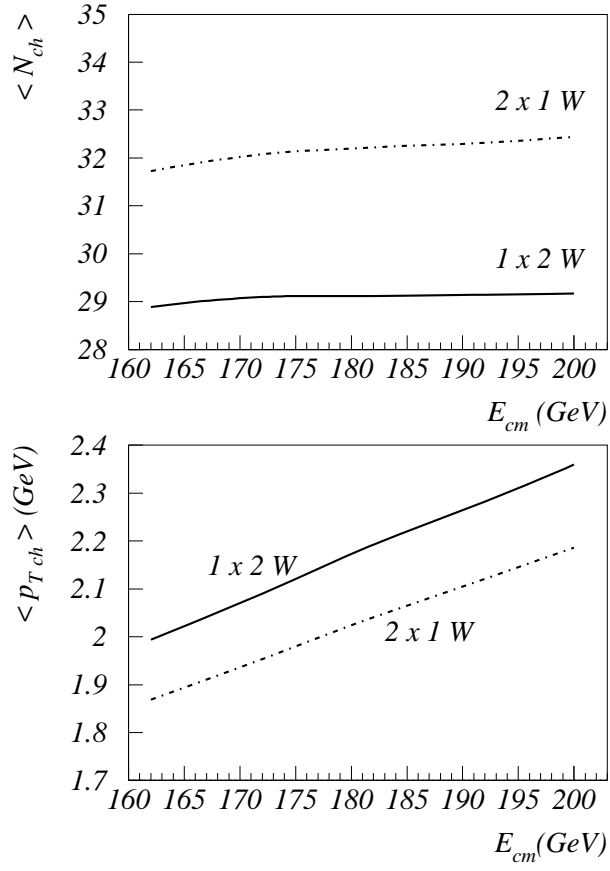


Figure 23: Possible differences between charged-hadron multiplicities and transverse momenta in $e^+e^- \rightarrow W^+W^- \rightarrow (\bar{q}q)(\bar{q}q)$ events ($1 \times 2W$) and independent $W^\pm \rightarrow (\bar{q}q)$ events ($2 \times 1W$).

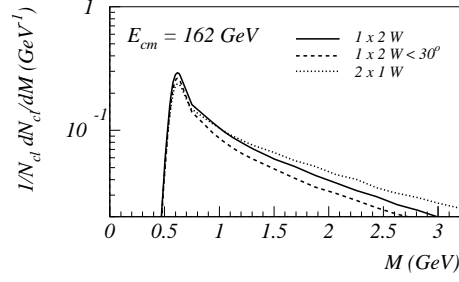


Figure 24: Cluster mass distributions in $W^+W^- \rightarrow (\bar{q}q)(\bar{q}q)$ (note the dependence on the angle between the decay dijets) and $W^\pm \rightarrow \bar{q}q$ events.

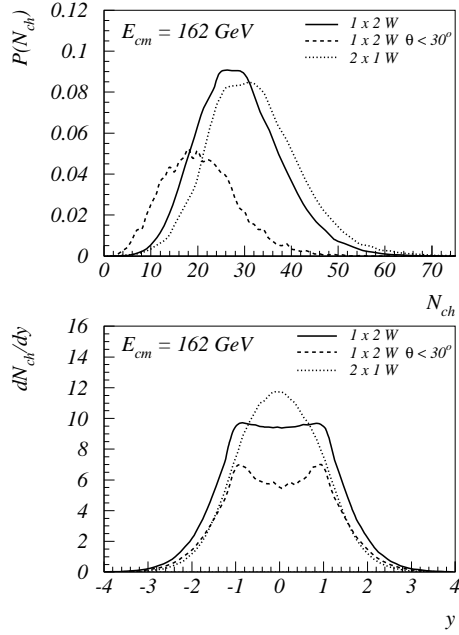


Figure 25: Hadron distributions in $W^+W^- \rightarrow (\bar{q}q)(\bar{q}q)$ (note again the angular dependence) and in $W^\pm \rightarrow \bar{q}q$ events.

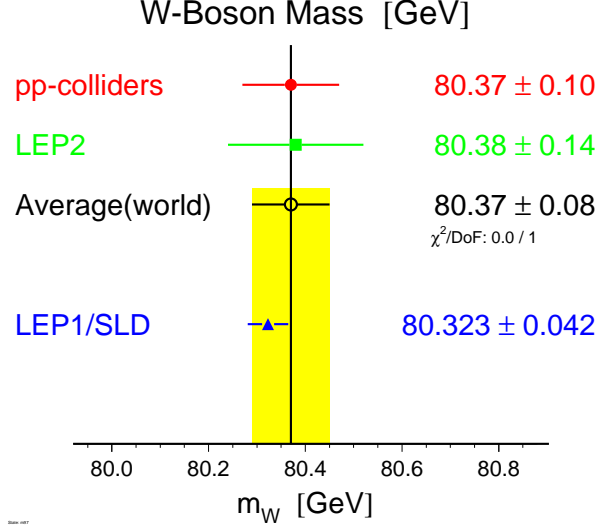


Figure 26: Compilation of direct measurements of m_W compared with prediction based on the Standard Model and precision electroweak measurements from LEP and the SLC.

2.4 TRIPLE-GAUGE COUPLINGS

The general form of WWV vertex, where $V = \gamma, Z$, may be parametrized as follows¹:

$$\begin{aligned}
& g_1^\nu V^\mu (W_{\mu\nu}^- W^{+\nu} - W_{\mu\nu}^+ W^{-\nu}) + \kappa_\nu W_\mu^+ W_\nu^- V^{\mu\nu} \\
& + \frac{\lambda_\nu}{m_W^2} V^{\mu\nu} W_\nu^{+\rho} W_{\rho\mu}^- + i g_5^\nu \epsilon_{\mu\nu\rho\sigma} ((\partial^\rho W^{-\mu}) W^{+\nu} - W^{-\mu} (\partial^\rho W^{+\nu})) V^\sigma \\
& + i g_4^\nu W_\mu^- W_\nu^+ (\partial^\mu V^\nu - \partial^\nu V^\mu) \\
& - \frac{\tilde{\kappa}_\nu}{2} W_\mu^- W_\nu^+ \epsilon^{\mu\nu\rho\sigma} \cdot V_{\rho\sigma} - \frac{\tilde{\lambda}_\nu}{2 m_W^2} W_{\rho\mu}^- W_\nu^{+\mu} \epsilon^{\nu\rho\alpha\beta} V_{\alpha\beta}
\end{aligned} \tag{2.22}$$

Electromagnetic gauge invariance imposes the restrictions $g_1^\gamma = 1$, $g_5^\gamma = 0$ at zero momentum $q^2 = 0$, with possible deviations at non-zero momentum transfers. In the Standard Model, one has¹

$$g_1^Z = g_1^\gamma = \kappa_Z = \kappa_\gamma = 1 \tag{2.23}$$

whilst the other couplings vanish. More generally, the coupling g_5^V violates C, P but conserves CP, whereas g_4^V , $\tilde{\kappa}_V$, $\tilde{\lambda}_V$ violate CP. For the remainder of

this short discussion, we assume C and P invariance, and make the following convenient multipole parametrization of the remaining terms¹

$$\begin{aligned} Q_W &= e g_1^\gamma, \quad \mu_W = \frac{e}{2m_W} (g_1^\gamma + \kappa_\gamma + \lambda_\gamma) \\ q_W &= -\frac{2}{m_W^2} (\kappa_\gamma - \lambda_\gamma) . \end{aligned} \quad (2.24)$$

Furthermore, it is plausible to assume an $SU(2) \times U(1)$ gauge-invariant parametrization, based on a linear realization, with a single Higgs doublet¹

$$\begin{aligned} & \frac{ig'}{m_W^2} \alpha_{B\phi} (D_\mu \Phi)^\dagger B^{\mu\nu} (D_\nu \Phi) + \frac{ig}{m_W^2} \alpha_{W\phi} (D_\mu \Phi)^\dagger \underline{\tau} \cdot \underline{W}^{\mu\nu} (D_\nu \Phi) \\ & + \frac{g}{6m_W^2} \alpha_W \underline{W}_\nu^\mu \cdot (\underline{W}_\rho^\nu \times \underline{W}_\mu^\rho) \end{aligned} \quad (2.25)$$

Thus we finally boil the fourteen parameters of Eq. (2.22) down to the three manageable parameters

$$\begin{aligned} \alpha_{W\phi} &= C_W^2 (g_1^Z - 1) \\ \alpha_{W\phi} + \alpha_{B\phi} &= -\frac{C_W^2}{S_W^2} (\kappa_Z - g_1^Z) = \kappa_\gamma - 1 \\ \alpha_W &= \lambda_\gamma = \lambda_Z \end{aligned} \quad (2.26)$$

which are used in most experimental analyses.

Since any one of these parameters leads to a non-renormalizable growth of $\sigma(e^+e^- \rightarrow W^+W^-)$ at high energies, they can only be effective low-energy parameters in a theory that is cut off at some higher-energy scale Λ_U . The possible magnitudes of these parameters depend on this scale Λ_U :

$$|\alpha_W| \simeq 19 \left(\frac{m_W}{\Lambda_\nu} \right)^2, \quad |\alpha_{W\phi}| \simeq 15.5 \left(\frac{m_W}{\Lambda_\nu} \right)^2, \quad |\alpha_{B\phi}| \simeq 49 \left(\frac{m_W}{\Lambda_\nu} \right)^2 \quad (2.27)$$

There are direct bounds on these parameters from the CDF and D0 experiments at the Fermilab Tevatron collider⁴⁵, as well as from LEP 2³. As was already discussed, cross-section measurements close to threshold are relatively insensitive to the triple-gauge couplings, and one can expect much more stringent bounds as LEP 2 advances to higher energies and luminosities^c.

^cIt should also be noted that there are indirect constraints on some combinations of triple-gauge couplings from their virtual effects on observables at LEP 1.

3 Supersymmetry and LEP 2

3.1 (S)Experimental demotivation

In the summer of 1995, there was considerable excitement around the apparently anomalous decay rates $Z \rightarrow \bar{b}b, \bar{c}c$: the first of these deviated from the prediction of the Standard Model by more than $3\frac{1}{2}\sigma$, and the latter disagreed by about $2\frac{1}{2}\sigma$. Even if one set R_c to its Standard Model value, R_b still differ from the Standard Model by 3σ ⁴⁶. There were many warnings that these were the most difficult of all the LEP 1 measurements, being dominated by systematic errors, but this did not stop theorists from speculating that the apparent discrepancies that might find origins in possible physics beyond the Standard Model.

In particular, two possible supersymmetric explanations were proposed⁴⁷. One involved a light pseudoscalar Higgs A and a very large value of $\tan\beta$, and the other involved light charginos χ^\pm and a light stop \tilde{t} , and a small value of $\tan\beta$, which were favoured in some models with an infra-red fixed point. Enthusiasm for this latter scenario raised hopes that the χ^\pm and \tilde{t} , might be detectable in the LEP 2 energy range.

As you know, this has not yet happened, implying that the supersymmetric contribution to R_b cannot be as large as had been speculated. Already the non-observation of supersymmetric particles at LEP 1.5, combined with other phenomenological considerations, indicated that supersymmetric particles could only provide a small part of the possible experimental discrepancy in R_b ⁴⁸. We implemented the available experimental constraints on $Z \rightarrow$ nothing visible, $Z \rightarrow \chi\chi'$, the requirements that $m_{\chi^\pm} \gtrsim m_Z/2$ and $m_h \gtrsim 40$ GeV, the CLEO constraint $B(b \rightarrow s\gamma) = (1 \text{ to } 4) \times 10^{-4}$, the CDF upper limit on non-Standard Model decays of the top quark, and D0 limits on the stop and neutralino masses. Finally, we implemented the LEP 1.5 limit on charginos: $m_{\chi^\pm} \gtrsim 65$ GeV if $m_{\chi^\pm} - m_\chi \gtrsim 10$ GeV.

We generated 365,000 choices of model parameters with $1 < \tan\beta < 5$ and 91,000 more in the restricted range $1 < \tan\beta < 1.5$, with supersymmetric mass parameters in the range $0 < \tilde{m} < 250$ GeV. We found only a handful of models that made a contribution to $R_b > 0.0010$, and we found the absolute upper limit⁴⁸

$$\Delta R_b < 0.0017 \tag{3.1}$$

We concluded that "... it may be necessary to review carefully the calcula-

tion and simulation of the Standard Model contributions to R_b and related measurements.”.

New experimental data became available during 1996, and the experimental discrepancy in R_b and R_c was much diminished to about 2σ ³. We revisited the calculation of supersymmetric contributions to R_b in the light of the new exclusions of supersymmetric parameter space from higher-energy LEP 2 runs⁴⁹. We implemented the LEP 1, CLEO and CDF constraints as before, and implemented the new limits on the lighter stop mass $m_{\tilde{t}}$ from LEP 2 and D0, and new limits on charginos from LEP 2: $m_{\chi^\pm} > 84$ GeV if $m_{\chi^\pm} - (m_{\tilde{\nu}} \text{ or } m_\chi)$ are greater than 3 GeV. However, we relaxed the previous limits on m_h , as a way of allowing larger values of the heavy second stop mass $m_{\tilde{t}_2}$.

Following our previous procedure, we generated 484,000 choices of supersymmetric model parameters, of which 10,000 gave $\Delta R_b > 0.0020$. After implementation of the constraints listed above, 41,000 models survived, of which 210, i.e., 0.04 % of the original sample, have $\Delta R_b > 0.0010$. This emphasizes the fact that large supersymmetric contributions to R_b are very special⁴⁹. Coincidentally, we found a maximum supersymmetric contribution $\Delta R_b \sim 0.0017$ again. However, we emphasized that such a large contribution to R_b required choices of parameters that were not attainable in conventional supergravity models, which could only yield⁴⁹

$$\Delta R_b < 0.0003 \quad (3.2)$$

a truly negligible contribution to resolving any residual discrepancy in R_b .

The reason for this can be understood from Fig. 27, which shows the projection on the (μ, M_2) plane of the “globular cluster” of surviving supersymmetric models, compared with the regions of this plane that are accessible in conventional supergravity models. This point is also made in Fig. 28, which shows a similar feature in the $(\theta_t, m_{\tilde{t}_1})$ plane characterizing stop mixing: the supergravity models miss entirely the interesting projection of the “globular cluster”. Moreover, we see in Fig. 29 that the surviving models are very vulnerable to small improvements in the current experimental exclusion domains in the $(m_{\tilde{t}_1}, m_\chi)$ plane. Indeed, about a half of the “globular cluster” has already been excluded by an improved limit from the OPAL collaboration⁵⁰ subsequent to our analysis^d.

^dThe apparent ability of supergravity models to reach into the “globular cluster” is only an artefact of this particular planar projection: as we saw in the previous figures 27 and 28, supergravity models are far away in other projections.

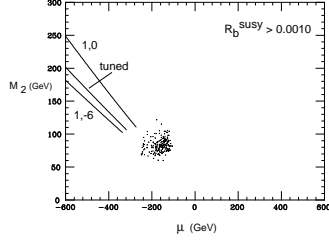


Figure 27: The “globular cluster” of surviving supersymmetric models with $\Delta R_b > 0.0010$, projected on the (μ, M_Z) plane and compared with the corresponding projection for favoured supergravity models.

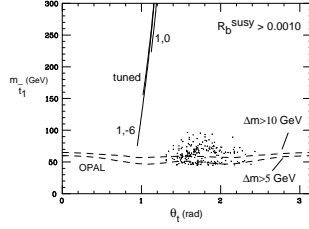


Figure 28: As for Fig. 27, but projected on the plane (θ_t, m_{t_1}) of \tilde{t} mixing parameters.

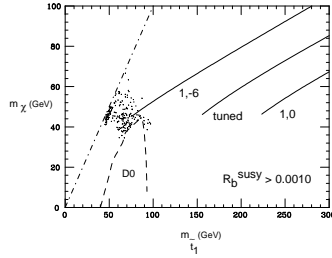


Figure 29: As for Fig. 27, but projected on the (m_{t_1}, m_χ) plane. Note that none of the favoured supergravity models crosses the “globular cluster” in the other projections shown in Figs. 27 and 28.

3.2 Lightest Supersymmetric Particle?

In many supersymmetric models, this is expected to be stable, and so should be present in the Universe today as a cosmological relic from the Big Bang. This stability would be the consequence of the multiplicatively-conserved quantum number called R parity⁵¹, which takes the value +1 for all conventional particles and -1 for all their supersymmetric partners. The conservation of R parity is related to those of baryon (B) and lepton (L) numbers:

$$R = (-1)^{3B+L+2S} \quad (3.3)$$

where S is the spin, which must be absolutely conserved! Violation of R conservation is possible if the model violates lepton or baryon number, either spontaneously or explicitly. If R parity is indeed conserved, we have the following three important consequences:

- Sparticles are always produced in pairs, e.g., $\bar{p}p \rightarrow \tilde{q}\tilde{g}X$, $e^+e^- \rightarrow \tilde{\mu}^+\tilde{\mu}^-$,
- Heavier sparticles decay into lighter ones, e.g., $\tilde{q} \rightarrow q\tilde{g}$, $\tilde{\mu} \rightarrow \mu\tilde{\gamma}$,
- The lightest supersymmetric particle is stable, because it has no legal decay mode.

However, this is just one of the possibilities for the lightest supersymmetric particle, as seen in Fig. 30. For example, if R parity is not conserved, even the lightest supersymmetric particle may decay into leptons and/or jets, a possibility that has excited renewed interest in the light of the recent large- q^2 events from HERA^{4,5}. If R parity is conserved, one can ask whether the lightest supersymmetric particle should be neutral, or whether it could have either electromagnetic and/or strong interactions. In the latter case, it would interact with ordinary matter and bind to form anomalous heavy isotopes which are not seen by experiment. Therefore, a stable LSP is presumably neutral with only weak interactions⁵², and the conventional candidate has been the lightest neutralino, as discussed below. In this case, supersymmetry has the “classic” pure missing-energy signature. Alternatively, the lightest neutralino might be heavier than some other supersymmetric particle, such as the gravitino \tilde{G} , in which case one would have the γ + missing-energy signature due to the decay $\tilde{\gamma} \rightarrow \gamma\tilde{G}$. We will now analyze each of these possibilities in turn.

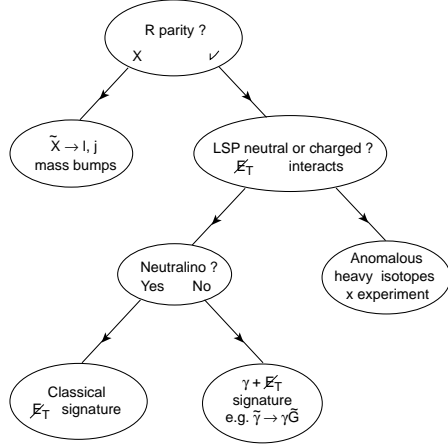


Figure 30: Flow chart of possible scenarios for the Lightest Supersymmetric Particle (LSP).

3.3 Constraints on a Stable Neutralino

The 2×2 chargino and 4×4 neutralino mass matrices of the MSSM are characterized at the tree level by common parameters: $SU(2)$ and $U(1)$ gaugino masses $M_{2,1}$, the Higgs mixing parameter μ and the ratio $\tan\beta \equiv v_1/v_2$ of Higgs vacuum expectation values. The chargino mass matrix is^{52,25}

$$\begin{pmatrix} M_2 & g_2 \frac{v_2}{\sqrt{2}} \\ \frac{g_2 v_1}{\sqrt{2}} & \mu \end{pmatrix} \quad (3.4)$$

with two mass eigenstates χ^\pm, χ'^\pm , and the neutralino mass matrix is^{52,25}

$$\begin{pmatrix} M_2 & 0 & \frac{-g_2 v_2}{\sqrt{2}} & \frac{g_2 v_1}{\sqrt{2}} \\ 0 & M_1 & \frac{g' v_2}{\sqrt{2}} & \frac{-g' v_1}{\sqrt{2}} \\ \frac{-g_2 v_2}{\sqrt{2}} & \frac{-g' v_2}{\sqrt{2}} & 0 & \mu \\ \frac{g_2 v_1}{\sqrt{2}} & \frac{-g' v_1}{\sqrt{2}} & \mu & 0 \end{pmatrix} \quad (3.5)$$

with four mass eigenstates χ_i . Gaugino mass universality $M_3 = M_2 = M_1 = m_{1/2}$ is often assumed at the grand unification scale, so that

$$\frac{M_2}{M_1} \simeq \frac{\alpha_2}{\alpha_1} = \frac{8}{3 \sin^2 \theta_W} \quad (3.6)$$

at the electroweak scale. Other supersymmetric model parameters enter when one discusses the production and decays of charginos and neutralinos, their annihilation in the early Universe and their scattering off nuclei. These include the scalar masses

$$\tilde{m}_i^2 = m_{0_i}^2 + C_i m_{1/2}^2 + \mathcal{O}(m_Z^2) \quad (3.7)$$

where the coefficients C_i are calculable using the renormalization group, and the m_{0_i} are soft supersymmetry-breaking scalar masses, that may (or may not) be universal at the GUT scale, as well as the physical Higgs boson masses. The latter may be characterized by one additional mass parameter m_A at the tree level, but are subject to important radiative corrections that depend in particular on m_t and the $m_{\tilde{t}_i}$, as discussed in Section 1.3³⁰. There are also interesting radiative corrections to the chargino and neutralino masses⁵³, as we discuss later, which may be neglected in a first approximation.

Important constraints on chargino and neutralino masses are imposed by searches for $e^+e^- \rightarrow \chi^+\chi^-$ and $\chi_i\chi_j$ at LEP 1 (in Z decays) and at higher energies. Neither the LEP 1 nor the LEP 1.5 data by themselves provided an absolute lower limit on the possible mass of the lightest neutralino χ . However, as seen in Fig. 31, the LEP 1.5 data filled in some wedges of the (μ, M_2) plane left uncovered by the LEP 1 data for $\mu < 0$ and $\tan\beta \lesssim 2$, at least for large $m_{\tilde{\nu}} \gtrsim 200$ GeV, enabling the absolute lower limit $m_\chi \geq 12.8$ GeV to be established⁵⁴, as seen in Fig. 32. However, there were loopholes in this first purely experimental analysis. One appeared for $\tan\beta \sim \sqrt{2}$ and $m_0 \sim 60$ GeV, when the decay $\chi^\pm \rightarrow \tilde{\nu} + e^\pm$ provided a soft lepton that was difficult to detect, diminishing the χ^\pm detection efficiency. There was also a very small loophole for $1 < \tan\beta < 1.02$, even at large $m_{\tilde{\nu}}$, that could probably be filled in by other LEP data.

We pointed out⁵⁵ that these loopholes could be plugged, and the lower limit on m_χ strengthened, by including other experimental constraints, as well as considerations based on cosmology, astrophysics and dynamical electroweak symmetry breaking, at the price of some assumptions of universality of the m_{0_i} . Neutrino counting at the Z peak tells us that $m_{\tilde{\nu}} > 43.1$ GeV if all three sneutrino species are degenerate, and LEP 1.5 searches for charged sleptons already told us that $m_{\tilde{\ell}^\pm} \gtrsim 45$ to 60 GeV, although these did not exclude $\chi^\pm \rightarrow \tilde{\nu} + \text{soft } \ell^\pm$ decay. However, upper limits on $e^+e^- \rightarrow \gamma + \text{nothing}$ from lower-energy accelerators, notably TRISTAN at KEK⁵⁶, excluded a domain of the $(m_0, m_{1/2})$ plane that ruled $m_\chi = 0$ out in the region $\tan\beta \sim \sqrt{2}$, $m_0 \sim 60$ GeV. Further constraints on $(m_0, m_{1/2})$ were obtained if one further assumed that the cosmological relic density of neutralinos $\rho_\chi = \Omega_\chi \rho_c$, where ρ_c is the

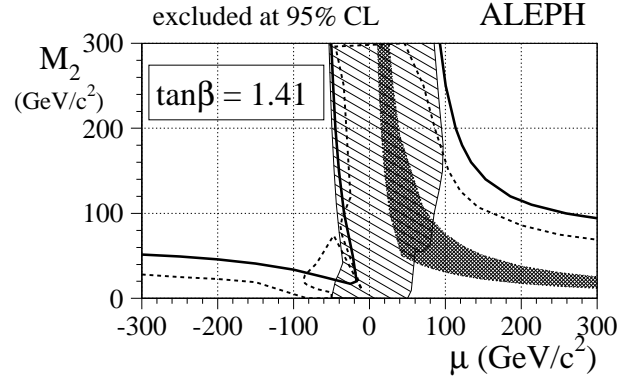


Figure 31: Interplay of gaugino constraints from LEP 1 (dashed line) and LEP 1.5 (thick solid line: $\chi^+\chi^-$, thin solid line $\chi\chi'$). Notice their complementarity in the $\mu < 0$ quadrant.

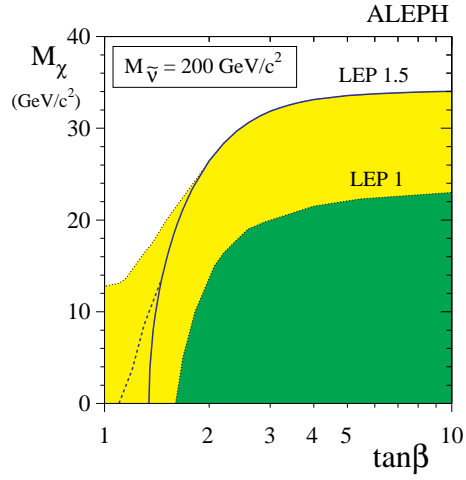


Figure 32: Experimental lower limit on m_χ , assuming a large sneutrino mass $m_{\tilde{\nu}} = 200 \text{ GeV}$ and ignoring a small loophole for $1.00 < \tan\beta < 1.02$. There is another, larger, loophole if $m_{\tilde{\nu}} \simeq 60 \text{ GeV}$ and $\tan\beta \simeq \sqrt{2}$.

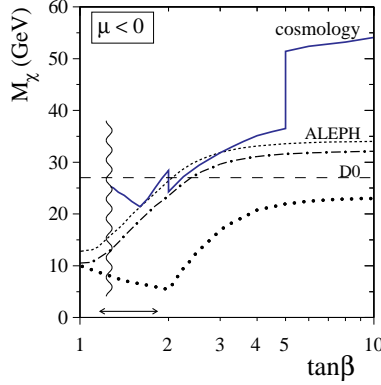


Figure 33: Phenomenological lower limits on m_χ based on LEP 1.5 data, for arbitrary m_0 , including the AMY result (dotted line), inferred from the $D\phi$ gluino search assuming universal gaugino masses (dashed line), assuming scalar-mass universality (dot-dashed line), and applying the cosmological constraint (3.8) (solid line).

critical cosmological density, fell into the range

$$0.1 \leq \Omega_\chi h^2 \leq 0.3 \quad (3.8)$$

where h encodes the current Hubble expansion rate: $H_0 = 100 h \text{ km s}^{-1} M_{pc}^{-1}$. The upper limit (3.8) is an absolute requirement if $\Omega_{total} \leq 1$ and the age of the Universe $t_0 \geq 12 \text{ Gy}$, whereas the lower limit in (3.8) is merely a preference for the neutralino to have a relic density large enough to be of astrophysical relevance. Under these assumptions, we found that the limits $m_{1/2} \rightarrow 0$, $\mu \rightarrow 0$ could be excluded, and we found the lower limit⁵⁵

$$m_\chi \gtrsim 21.4 \text{ GeV} \quad (3.9)$$

occurring when $\tan \beta \simeq 1.6$, with m_χ necessarily much larger for generic values of $\tan \beta$, as seen in Fig. 33.

We have recently updated this analysis, including the latest chargino and neutralino limits from the higher-energy LEP 2W and LEP 2 runs, and exploring systematically the consequences of extending the universal scalar-mass assumption to more sfermion species⁵⁷. The primary experimental searches are those for $e^+e^- \rightarrow \chi^+\chi^-$, which enforce

$$m_{\chi^\pm} \gtrsim 85 \text{ GeV} \times f(\mu, m_{\tilde{\nu}}, \tan \beta) \quad (3.10)$$

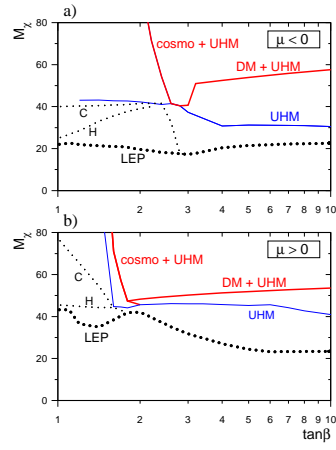


Figure 34: Lower limits on m_χ based on data from LEP 1, 1.5 and 2. The dotted line makes no appeal to extra theoretical assumptions. Lines labelled UHM assume universal scalar masses also for Higgs bosons. The branches labelled “cosmo” and “DM” assume the upper and lower limits in Eq. (3.8), respectively. The lines labelled C and H are explained in ⁵⁷.

and for $e^+e^- \rightarrow \tilde{e}^+\tilde{e}^-$, which impose

$$m_{\tilde{e}} \gtrsim 70 \text{ GeV} \times f(\mu, m_{1/2}, \tan \beta) \quad (3.11)$$

Assuming input slepton mass universality: $m_{\tilde{e}_R} = m_{\tilde{e}_L} = m_{\tilde{\nu}_L}$, the low- m_0 loophole is largely filled in, and the $\tan \beta < 1.02$ loophole completely disappears. Also of great importance are the LEP searches for $e^+e^- \rightarrow h + Z$. If one extends the universality assumption to the squarks, these provide important lower limits on $(m_{0_1}, m_{1/2})$, in order that the h boson be heavy enough to have escaped detection. These searches also tend to fill in the low- m_0 hole. Further strengthening of the lower limit on m_χ is found if one extends the scalar-mass universality assumption to the Higgs bosons. This assumption fixes μ and m_A as functions of the other parameters, refining the direct LEP search limits on charginos and sleptons, and enabling the search for $e^+e^- \rightarrow h + A$ to come into play. Finally, dramatic strengthening of the lower limit on m_χ is found at low $\tan \beta$ if one imposes the cosmological upper limit on $\Omega_\chi h^2$ (3.8). Combining these considerations, as seen in Fig. 34, we find⁵⁷

$$m_\chi \gtrsim 40 \text{ GeV} \quad (3.12)$$

whatever the value of $\tan \beta$, and also lower limits $\tan \beta \gtrsim 1.7$ if $\mu < 0$ and $\tan \beta \gtrsim 1.4$ if $\mu > 0$.

The latter results do not apply if one relaxes the scalar-mass universality assumption, enabling one to consider the possibility that the lightest neutralino is mainly a higgsino. This must weigh less than 80 GeV, otherwise it would annihilate into W^+W^- pairs in the early Universe, leaving an uninterestingly low relic density. On the other hand, in this region of parameter space LEP 2 searches would have observed $\chi^+\chi^-$ production if $m_{\chi^\pm} \lesssim 80$ GeV and $m_{\chi^\pm} - m_\chi \gtrsim 5$ GeV. We infer that there remains only a narrow window $80 \text{ GeV} \gtrsim m_{\chi^\pm} \gtrsim 75 \text{ GeV}$ for higgsino-like dark matter⁵⁷. Just where this region lies in the conventional (μ, M_2) plane depends sensitively on quantum corrections to m_{χ^\pm} and m_χ ⁵³, and hence on $\Omega_\chi h^2$ ⁵⁸, which is very sensitive to $m_{\chi^\pm} - m_\chi$. The interplay of theoretical, experimental and cosmological considerations in the presence of these quantum corrections merits deeper study. x

3.4 *R-Conserving Neutralino Decay?*

Decay of the lightest neutralino into a lighter sparticle, such as the gravitino \tilde{G} , is a generic possibility in no-scale supergravity models⁵⁹ in which

$$m_{\tilde{G}} = 0 \left(\left(\frac{m_W}{m_P} \right)^p \right) \quad m_P : p > 1 \quad (3.13)$$

is achievable, and in gauge-mediated “messenger” models of supersymmetry breaking⁶⁰. The radiative decay $\chi \rightarrow \gamma \tilde{G}$ would decay inside the experimental apparatus if $m_{\tilde{G}}$ is sufficiently small, producing a $\gamma\gamma + \cancel{E}_T$ signature from sparticle-pair production.

Interest in such models has been resuscitated by the (in)famous $\bar{p}p \rightarrow e^+e^-\gamma\gamma + \cancel{E}_T + X$ event reported by the CDF collaboration⁶¹. Among the possible interpretations are $\chi^+\chi^-$ pair production (with $m_{\chi^\pm} \lesssim 150$ GeV to get a large enough rate), followed by $\chi^\pm \rightarrow e^\pm \nu \gamma \tilde{G}$ decay, and $\tilde{e}^+\tilde{e}^-$ production (with $m_{\tilde{e}} \gtrsim 100$ GeV to get a large enough rate), followed by $\tilde{e}^\pm \rightarrow e^\pm \gamma \tilde{G}$ decay⁶².

These interpretations are significantly constrained by LEP 2 searches for $e^+e^- \rightarrow (\chi \rightarrow \gamma \tilde{G})(\chi \rightarrow \gamma \tilde{G})$ ⁶³. As seen in Fig. 35a, preliminary LEP 2W results already excluded a considerable fraction of the parameter space in the $\chi^+\chi^-$ interpretation of the CDF event, depending on the value of $m_{\tilde{e}^\pm}$ assumed. A large fraction of the parameter space in the $\tilde{\ell}^+\tilde{\ell}^-$ interpretation has also been excluded, as seen in Fig. 35b, and the fate of this option may be decided by future higher-energy LEP runs. Perhaps last week’s gravity-mediated models of supersymmetry breaking, with a heavy gravitino $m_{\tilde{G}} > m_\chi$, were not so bad after all?

3.5 *R Violation ?*

In addition to the Yukawa superpotential terms which give masses to the quarks and leptons, and to the Higgs mixing μ term, there are other superpotential terms allowed by the gauge symmetries of the MSSM⁶⁴:

$$\epsilon_i H L_i + \lambda_1^{ijk} L_i L_j E_k^c + \lambda'_{ijk} L_i Q_j D_k^c + \lambda''_{ijk} U_i^c D_j^c D_k^c \quad (3.14)$$

each of which violates lepton and/or baryon number, and hence R parity. The $H L_i$ mixing terms may be removed by a change in field basis, and the

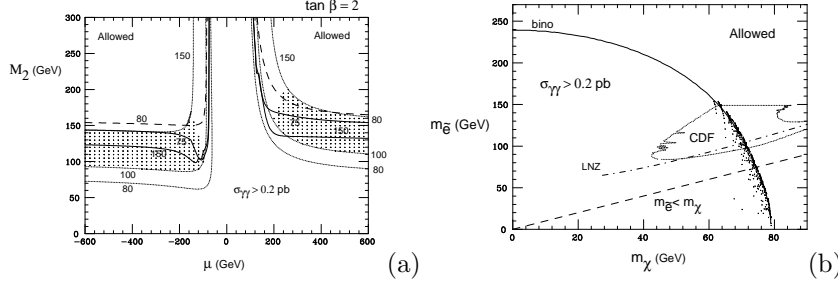


Figure 35: Parameter spaces of favoured light-gravitino models postulating (a) chargino (dotted regions) and (b) selectron (CDF “shark’s tooth”) decay to explain the CDF $e^+e^- \gamma\gamma \cancel{E}_T$ event, compared with preliminary LEP 2 constraints, (a) for different values of $m_{\tilde{e}}$, and (b) for different values of m_{χ} .

last two terms cannot be present simultaneously, as they would cause rapid baryon decay. Any of the three trilinear interactions in (3.14) would provide dramatic new decay signatures for sparticles: $\tilde{X} \rightarrow \ell\ell$, ℓq or qq . Indeed, R -violating models might even be easier to spot than the conventional R -conserving scenario. For example, the process $e^+e^- \rightarrow \chi\chi$ becomes observable at LEP because the lightest neutralino χ has visible decay modes.

R -violating models have been unfashionable for several reasons. One is that, since χ is unstable, it is no longer a good candidate for cold dark matter in the Universe. Another is that R -violating couplings would be strongly constrained by cosmology if the observed baryon asymmetry has a primordial origin^{65,66}. This is because the B - and/or L -violating interactions in (3.14), in conjunction with the $(B+L)$ -violating non-perturbative interactions in the Standard Model, would eradicate any primordial B or L asymmetry. Persistence of such an asymmetry would provide upper limits⁶⁷

$$\left| \frac{\epsilon_i}{\mu} \right| \lesssim 3 \times 10^{-6}, \quad |\lambda| \lesssim 10^{-7} \quad (3.15)$$

for generic flavour structures of R -violating couplings. However, it has been proposed that one might be able to evade these constraints by playing flavour-symmetry games, and the cosmological baryon asymmetry might have originated at the electroweak phase transition, obviating the bounds (3.15)^{65,68}. Another potential difficulty for R -violating models is the observed flavour conservation in neutral interactions, which is natural in the Standard Model but not in its known R -violating extensions.

Some phenomenological interest in R -violating models was sparked by the ALEPH report of a possible signal in $e^+e^- \rightarrow 4$ jets⁶⁹, interpretable as associated production of a pair of particles decaying into dijet pairs. The least implausible model for this observation that I know postulates the reaction $e^+e^- \rightarrow \tilde{e}_L^\pm \tilde{e}_R^\pm$, with both \tilde{e}^\pm decaying into $\bar{q}q$ via R -violating couplings⁷⁰. This could be compatible with the ALEPH data if $m_{\tilde{e}_R} \sim 48$ GeV, $m_{\tilde{e}_L} \sim 58$ GeV, and one chooses carefully other parameters of the model so as to avoid large cross-sections for $e^+e^- \rightarrow \tilde{\nu}_e \tilde{\nu}_e$ and/or $\chi\chi$ production. However, since the ALEPH signal has not been confirmed by the other LEP experiments⁷¹, interest in it has waned.

On the other hand, interest in R -violating models has waxed enormously after the report by the H1⁴ and ZEUS⁵ collaborations of a possible excess of $e^+p \rightarrow e^+qX$ events at large Q^2 . Superficially, the Q^2 distribution resembles more what one would expect from a direct-channel spin-0 resonance than a contact interaction⁷², and this is also suggested by the x measurements of the H1 collaboration⁴, which are more precise than those of ZEUS⁵. However, production of a non-supersymmetric leptoquark may be difficult to reconcile with limits established by the CDF collaboration⁷³, since its branching ratio into e^+q could only with difficulty be much less than unity.

Within supersymmetry the natural interpretation^{74,76,77,72,75} would use the λ'_{ijk} interaction in (3.14) to produce a charge-2/3 squark: $e_{d_{kR}}^+ \rightarrow \tilde{u}_{Lj}$. Production of $\tilde{u}_L/\tilde{c}_L/\tilde{t}$ off a valence d quark would require a coupling $|\lambda'_{1j1}| \sim 1/25$, whilst production off a sea s or b quark would require $|\lambda'_{1jk}| \sim 1/3$. Production of the \tilde{u}_L would conflict⁷² with the following upper bound from nuclear $\beta\beta$ decay⁷⁸:

$$|\lambda'_{111}| < 7 \times 10^{-3} \left(\frac{m_{\tilde{g}}}{200 \text{ GeV}} \right)^2 \left(\frac{m_{\tilde{g}}}{1 \text{ TeV}} \right)^{1/2} \quad (3.16)$$

whilst production of the \tilde{c}_L off the d quark is barely compatible with upper limits from searches for $K \rightarrow \pi \bar{\nu} \nu$ decay⁷². On the other hand, \tilde{t} production off either d or s quarks seems to be compatible with all known constraints⁷⁹.

One wants the branching ratio $B(\tilde{q} \rightarrow e^+q)$ not to be very small – in order that HI and ZEUS have a signal to see – and not too close to unity – otherwise CDF could have seen $\tilde{q}\tilde{q}$ pair production⁷³. In the case of $d \rightarrow \tilde{c}_L$ production, there can be significant competition between R -violating $\tilde{c}_L \rightarrow e^+d_R$ and R -conserving $\tilde{c}_L \rightarrow c\chi$ decays, despite the small λ'_{121} coupling, due to a possible cancellation in the R -conserving coupling between the different

gaugino components in the lightest neutralino χ ⁷²:

$$\frac{1}{2}g (N_{i2} + \frac{1}{3} \tan \theta_W N_{i2}) \quad (3.17)$$

The effect of this possible cancellation can be seen in Fig. 36 for $\mu > 0$. On the other hand, in the case of $d \rightarrow \tilde{t}$ production, there is only a very limited range of parameter space where $\tilde{t} \rightarrow e^+ d$ is competitive with R -conserving \tilde{t} decays⁷². The case of $s \rightarrow \tilde{t}$ production is intermediate between these two, in that competition between the R -conserving and -violating decays is possible if $m_{\tilde{t}} \gtrsim 210$ GeV, but more difficult for $m_{\tilde{t}} \lesssim 200$ GeV⁷⁹. In any of these scenarios, $\tilde{q} \rightarrow q\chi$ decays could provide an interesting alternative decay signature for either the HERA experiments or CDF⁷².

What about signatures at LEP 2? There could be effects on $\sigma(e^+e^- \rightarrow \bar{q}q)$ and/or the final-state angular distributions due to R -violating \tilde{q} exchange⁸⁰.

There could be single production $e^+e^- \rightarrow e^\pm \frac{(-)}{q} \tilde{q}$ if $m_{\tilde{q}} < E_{cm}$ ⁸¹. The reaction $e^+e^- \rightarrow \chi\chi$ would be detectable if $m_\chi < E_{cm}/2$. Also interesting would be a $L_i L_j E_k^c$ coupling: this could give interference effects or even a direct-channel $\tilde{\nu}$ resonance in $e^+e^- \rightarrow L^+ L^-$!⁸²

3.6 Supersymmetry at the LHC

This has recently been the subject of a workshop at CERN⁸³, and broad studies have been made by the ATLAS and CMS collaborations using complementary approaches. ATLAS has made detailed analyses of a few selected points in the multidimensional supersymmetric parameter space, and CMS has made a comprehensive scan. A key feature of these studies has been that the LHC produces many heavier sparticles that decay into lighter ones, and that these cascades can often be reconstructed efficiently⁸⁴. In general, the dominant signatures are jets + leptons + \cancel{E}_T , and the physics reach is large: $m_{\tilde{q},\tilde{g}} \rightarrow 2$ TeV, $m_{\tilde{\ell}} \rightarrow 400$ GeV, etc. Some examples of the reconstruction of lighter sparticles in the cascade decays are shown in Fig. 37. These will enable precision measurements of model parameters, within a given theoretical framework⁸⁴.

Table 4 shows the plethora of sparticles detectable at each of the five points in parameter space selected by ATLAS for special study. We see that the LHC may be able to find a large fraction of the expected sparticle Zoo⁸⁴. Remember that the Bevatron was built to find the antiproton (which it did), but is mainly famous for discovering the complicated hadron spectrum. Much

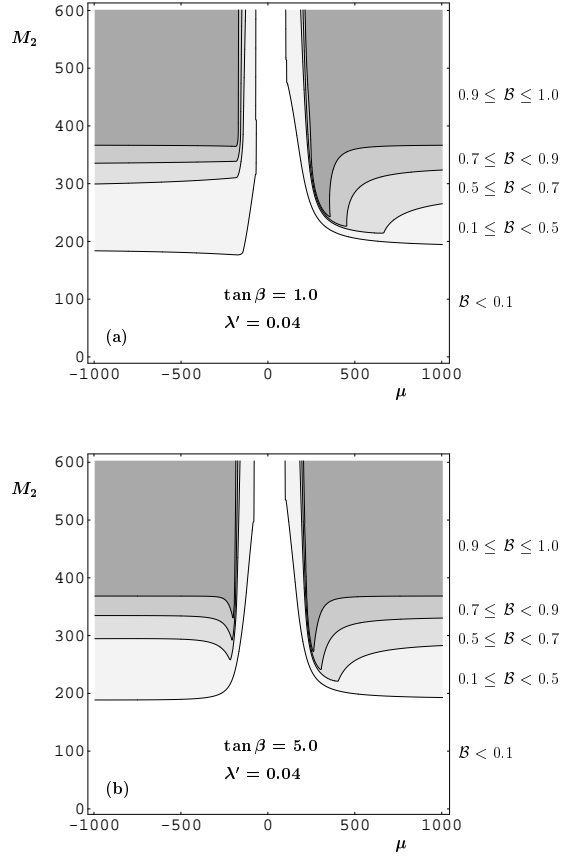


Figure 36: Branching ratio of $\tilde{c}_L \rightarrow c\chi$ decay in the $e^+d \rightarrow \tilde{c}_L$ R -violating squark interpretation of the HERA large- Q^2 data.

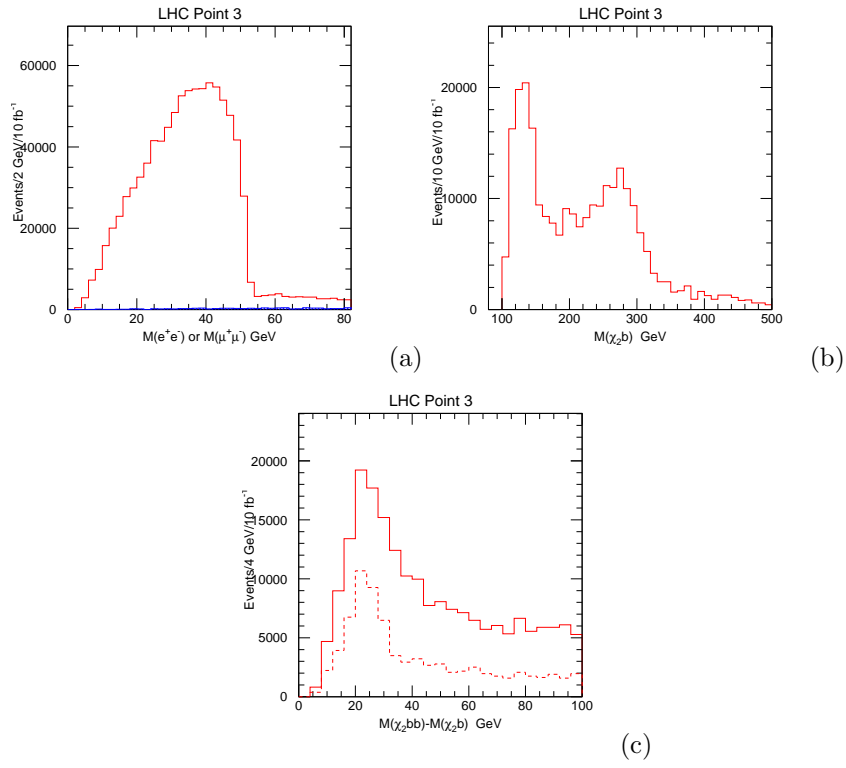


Figure 37: Reconstruction of sparticle masses for a particular supergravity model studied in (citehcsusy), demonstrating (a) the end-point in $\chi_2 \rightarrow \chi \ell^+ \ell^-$ decay, (b) the $\tilde{b} \rightarrow \chi_2 b$ mass bump, and (c) the $\tilde{g} \rightarrow b\bar{b}$ mass bump.

Table 4: The LHC as “Bevatrino”: Sparticles detectable at selectred points in supersymmetric parameter space are denoted by +

	h	H/A	χ_2^0	χ_3^0	χ_4^0	χ_1^\pm	χ_2^\pm	\tilde{q}	\tilde{b}	\tilde{t}	\tilde{g}	$\tilde{\ell}$
1	+		+					+	+	+	+	
2	+		+					+	+	+	+	
3	+	+	+			+		+	+		+	
4	+		+	+	+	+	+	+			+	
5	+		+					+	+	+	+	+

of the motivation for the LHC is to find the Higgs boson (which it can), but maybe it will become famous for finding sparticles – the LHC as “Bevatrino”?!

1. *Proceedings of the Workshop on Physics at LEP 2*, eds. G. Altarelli, T. Sjöstrand and F. Zwirner, CERN Report 96-01.
2. J. Ellis, M.K. Gaillard and D.V. Nanopoulos, *Nucl.Phys.* **B106** (1976) 292;
B.L. Ioffe and V.A. Khoze, *Sov.J.Part.Nucl.* **9** (1978) 50;
B.W. Lee, C. Quigg and H. Thacker, *Phys.Rev.Lett.* **38** (1977) 883 and *Phys.Rev.* **D16** (1977) 1519.
3. LEP Electroweak Working Group, CERN preprint PPE/97-183.
4. H1 Collaboration, *Z.Phys.* **C74** (1997) 191;
Y. Sirois, for the H1 Collaboration.
5. ZEUS Collaboration, *Z.Phys.* **C74** (1997) 207;
B. Straub, for the ZEUS Collaboration.
6. *Z Physics at LEP 1*, eds. G. Altarelli, R. Kleiss, and C. Verzegnassi, CERN report 89-08.
7. K.A. Olive, Lectures at this school, astro-ph/9707212.
8. D0 Collaboration, *Phys.Rev.Lett.* **77** (1996) 3309, and references therein.
9. L. Arnaudon et al., *Z.Phys.* **C66** (1995) 45.
10. J. Wenninger, CERN Preprint SL/TN Note 95-21(OP) (1995).
11. G. Wilkinson, Talk at the *International Conference on high Energy Physics*, Warsaw, 1996.
12. M. Veltman, *Nucl.Phys.* **B123** (1977) 89;
M.S. Chanowitz, M. Furman and I. Hinchliffe, *Phys.Lett.* **78B** (1978) 285.
13. M. Veltman, *Acta Phys.Pol.* **8** (1977) 475.
14. J. van der Bij and M. Veltman, *Nucl.Phys.* **B231** (1984) 205.

15. *Reports of the Working Group on Precision Calculations for the Z resonance*, eds. D. Bardin, W. Hollik and G. Passarino, CERN Report 95-03.
16. J. Ellis and G.L. Fogli, *Phys.Lett.* **B231** (1989) 189.
17. J. Ellis, G.L. Fogli and E. Lisi, *Phys.Lett.* **B389** (1996) 321.
18. R. Raja, for the CDF and D0 Collaborations, hep-ex/9706011.
19. C. Vayonakis, *Lett. Nuovo Cimento* **17** (1976) 383 and Athens University Preprint (1978);
B.W. Lee, C. Quigg and H.B. Thacker, *Phys.Rev.* **D16** (1977) 1519.
20. M. Lindner, *Z.Phys.* **C31** (1986) 295.
21. P. Hasenfratz and J. Nager, *Z.Phys.* **C37** (1988) 477.
22. M. Sher, *Physics Reports* **179** (1989) 273.
23. Y.A. Gol'fand and E.P. Likhtman, *Pis'ma Zh.E.T.F.* **13** (1971) 323;
D. Volkov and V.P. Akulov, *Phys.Lett.* **46B** (1973) 109;
J. Wess and B. Zumino, *Nucl.Phys.* **B70** (1974) 39;
for a review, see P. Fayet and S. Ferrara, *Physics Reports* **32C** (1977) 249.
24. L. Maiani, *Proceedings Summer School on Particle Physics*, Gif-sur-Yvette, 1979 (IN2P3, Paris, 1980), p. 3;
G. 't Hooft, in *Recent Developments in Field Theories*, eds. G. 't Hooft et al. (Plenum Press, New York, 1980);
E. Witten, *Nucl.Phys.* **B188** (1981) 513;
R.K. Kaul, *Phys.Lett.* **109B** (1982) 19.
25. For reviews, see: H.P. Nilles, *Physics Reports* **110** (1984) 1;
H.E. Haber and G.L. Kane, *Physics Reports* **117** (1995) 75.
26. J. Ellis, K. Enqvist, D.V. Nanopoulos and F. Zwirner, *Mod.Phys.Lett.* **A1** (1986) 57.
27. R. Barbieri and G.F. Giudice, *Nucl.Phys.* **B306** (1988) 63.
28. S. Dimopoulos and G.F. Giudice, *Phys.Lett.* **B357** (1995) 573.
29. S. Dimopoulos, S. Raby and F. Wilczek, *Phys.Rev.* **D24** (1981) 1681;
W.J. Marciano and G. Senjanovic, *Phys.Rev.* **D25** (1982) 3092;
L.E. Ibáñez and G.G. Ross, *Phys.Lett.* **105B** (1982) 439;
M.B. Einhorn and D.R.T. Jones, *Nucl.Phys.* **B196** (1982) 475;
J. Ellis, S. Kelley and D.V. Nanopoulos, *Phys.Lett.* **B249** (1990) 441 and **B260** (1991) 131;
P. Langacker and M. Luo, *Phys.Rev.* **D44** (1991) 817;
U. Amaldi, W. de Boer and H. Furstenau, *Phys.Lett.* **B260** (1991) 447;
F. Anselmo, L. Cifarelli, A. Petermann and A. Zichichi, *Nuovo Cimento* **104A** (1991) 1817.
30. Y. Okada, M. Yamaguchi and T. Yanagida, *Progr.Theor.Phys.* **85** (1991)

- 1;
- J. Ellis, G. Ridolfi and F. Zwirner, *Phys.Lett.* **B257** (1991) 83; *Phys.Lett.* **B262** (1991) 477;
- H.E. Haber and R. Hempfling, *Phys.Rev.Lett.* **66** (1991) 1815;
- R. Barbieri, M. Frigeni and F. Caravaglios, *Phys.Lett.* **B258** (1991) 167;
- Y. Okada, M. Yamaguchi and T. Yanagida, *Phys.Lett.* **B262** (1991) 54.
31. M. Carena, M. Quiros and C.E.M. Wagner, *Nucl.Phys.* **B461** (1996) 407;
- H.E. Haber, R. Hempfling and A.H. Hoang, hep-ph/9609331.
32. D.R.T. Jones and S.T. Petcov, *Phys.Lett.* **84B** (1979) 440.
33. E. Richter-Was, D. Froidevaux, F. Gianotti, L. Poggioli, D. Cavalli and S. Resconi, CERN Preprint TH/96-111 (1996).
34. ALEPH Collaboration, CERN preprint PPE/97-070.
35. ALEPH Collaboration, CERN preprint PPE/97-071
36. Yu.L. Dokshitzer, V.A.Khoze, L.H. Orr and W.J. Stirling, *Nucl.Phys.* **B403** (1993) 65;
- V.S. Fadin, V.A. Khoze and A.D. Martin, *Phys.Lett.* **B320** (1994) 141;
- Phys.Rev.* **D49** (1994) 2247;
- G. Gustafson, U.Pettersson and P. Zerwas, *Phys.Lett.* **B209** (1988) 90;
- T. Sjöstrand and V.A. Khoze, *Phys.Rev.Lett.* **72** (1994) 28; *Z.Phys.* **C62** (1994) 281;
- G. Gustafson and J. Häkkinen, *Z.Phys.* **C64** (1994) 659.
37. L. Lönnblad and T. Sjöstrand, *Phys.Lett.* **B351** (1995) 293.
38. J. Ellis and K. Geiger, *Phys.Rev.* **D52** (1995) 1500; *Nucl.Phys.* **A590** (1995) 609.
39. J. Ellis and K. Geiger, *Phys.Rev.* **D54** (1996) 1755.
40. J. Ellis and K. Geiger, CERN preprint TH/97-46, hep-ph/9703348.
41. V.S. Fadin, V.A. Khoze, A.D. Martin and W.J. Stirling, *Phys.Lett.* **B363** (1995) 112, and references therein.
42. K. Geiger, *Phys.Rev.* **D54** 949 (1996); preprint BNL-63087, hep-ph/9611400.
43. B.A. Campbell, J.Ellis and K.A. Olive, *Phys.Lett.* **B325** (1990) 325 and *Nucl.Phys.* **B345** (1990) 57.
44. DELPHI Collaboration, CERN preprint PPE/97-030.
45. CDF Collaboration, *Phys.Rev.Lett.* **78** (1997) 4536;
- D0 Collaboration, hep-ex/9705010.
46. LEP Electroweak Working Group, CERN preprint PPE/95-172.
47. A. Djouadi et al., *Nucl.Phys.* **B349** (1991) 48;
- M. Boulware and D. Finell, *Phys.Rev.* **D44** (1991) 2054;
- G. Altarelli, R. Barbieri and F. Caravaglios, *Phys.Lett.* **B314** (1993)

- 357;
D. Garcia and J. Sola, *Phys.Lett.* **B357** (1995) 349;
X. Wang, J. Lopez and D.V. Nanopoulos, *Phys.Rev.* **D52** (1995) 4116;
M. Shifman, *Mod.Phys.Lett.* **A10** (1995) 605;
G.L. Kane, R.G. Stuart and J.D. Wells, *Phys.Lett.* **B354** (1995) 350;
J. Erler and P. Langacker, *Phys.Rev.* **D52** (1995) 441;
P.H. Chankowski and S. Pokorski, *Nucl.Phys.* **B475** (1996) 3.
48. J. Ellis, J.J. Lopez and D.V. Nanopoulos, *Phys.Lett.* **B372** (1996) 95.
49. J. Ellis, J.L. Lopez and D.V. Nanopoulos, *Phys.Lett.* **B397** (1997) 88.
50. OPAL Collaboration, CERN preprint PPE/97-046.
51. P. Fayet, in *Unification of the Fundamental Particle Interactions*, eds. S. Ferrara, J. Ellis and P. van Nieuwenhuizen (Plenum Press, New York, 1980), p. 587.
52. J. Ellis, J.S. Hagelin, D.V. Nanopoulos, K.A. Olive and M. Srednicki, *Nucl.Phys.* **B238** (1984) 453.
53. G.F. Giudice and A. Pomarol, *Phys.Lett.* **B372** (1996) 253.
54. ALEPH Collaboration, D. Buskulic et al., *Z.Phys.* **C72** (1996) 549.
55. J. Ellis, T. Falk, K.A. Olive and M. Schmitt, *Phys.Lett.* **B388** (1996) 97.
56. AMY Collaboration, Y. Sugimoto et al., *Phys.Lett.* **B369** (1996) 86.
57. J. Ellis, T. Falk, K.A. Olive and M. Schmitt, CERN preprint TH/97-105, hep-ph/9705444.
58. M. Drees, M.M. Nojiri, D.P. Roy and Y. Yamada, *Phys.Rev.* **D56** (1997) 276.
59. J. Ellis, K. Enqvist and D.V. Nanopoulos, *Phys.Lett.* **B147** (1984) 99; *Phys.Lett.* **B151** (1985) 357.
60. See, e.g., M. Dine and A. Nelson, *Phys.Rev.* **D48** (1993) 1277, **D51** (1995) 1362 and **D53** (1996) 2658.
61. S. Park, in *Proceedings of the 10th Topical Workshop on Proton-Antiproton Collider Physics*, Fermilab, 1995, eds. R. Raja and J. Yoh (AIP, New York, 1995), p. 62.
62. D. Stump, M. Wiest and C.-P. Yuan, *Phys.Rev.* **D54** (1996) 1936;
S. Dimopoulos, M. Dine, A. Raby and S. Thomas, *Phys.Rev.Lett.* **76** (1996) 3494;
S. Ambrosanio, G. Kane, G. Kribs, S. Martin and S. Mrenna, *Phys.Rev.Lett.* **76** (1996) 3498 and *Phys.Rev.* **D54** (1996) 5395;
S. Dimopoulos, S. Thomas and J. Wells, *Phys.Rev.* **D54** (1996) 3283;
K. Babu, C. Kolda and F. Wilczek, *Phys.Rev.Lett.* **77** (1996) 3070;
J.L. Lopez and D.V. Nanopoulos, *Mod. Phys. Lett.* **A10** (1996) 2473 and *Phys.Rev.* **D55** (1997) 4450;

- J.L. Lopez, D.V. Nanopoulos and A. Zichichi, *Phys.Rev.Lett.* **77** (1996) 5168 and *Phys.Rev.* **D55** (1997) 5813.
63. J. Ellis, J.L. Lopez and D.V. Nanopoulos, *Phys.Lett.* **B394** (1997) 354.
64. See, for instance, the following papers and references therein:
 G. Bhattacharyya, D. Choudhury and K. Sridhar, *Mod.Phys.Lett.* **A10** (1995) 1583 and *Phys.Lett.* **B355** (1995) 193;
 C.E. Carlson, P. Roy and M. Sher, *Phys.Lett.* **B357** (1995) 99;
 M. Hirsch, H.V. Klapdor-Kleingrothaus and S.G. Kovalenko, *Phys.Rev.Lett.* **75** (1995) 17;
 K.S. Babu and R.N. Mohapatra, *Phys.Rev.Lett.* **75** (1995) 2276;
 A.Yu. Smirnov and F. Vissani, IC-96-16, hep-ph/9601387;
 D. Choudhury and P. Roy, *Phys.Lett.* **B378** (1996) 153;
 M. Chaichian and K. Huitu, *Phys.Lett.* **B384** (1996) 157;
 H. Nunokawa, A. Rossi and J.W.F. Valle, *Nucl.Phys.* **B482** (1996) 481.
65. B.A. Campbell, S. Davidson, J. Ellis and K.A. Olive, *Phys.Lett.* **B256** (1991) 457; *Astroparticle Phys.* **1** (1992) 77.
66. W. Fischler, G.F. Giudice, R.G. Leigh and S. Paban, *Phys.Lett.* **B258** (1991) 45.
67. S. Davidson and J. Ellis, *Phys.Lett.* **B390** (1997) 210 and CERN preprint TH/97-004, hep-ph/9702247.
68. H. Dreiner and G.G. Ross, *Nucl.Phys.* **B410** (1993) 188.
69. D. Buskulic et al., ALEPH Collaboration, *Z.Phys.* **C71** (1996) 179;
 G. Cowan, for the ALEPH Collaboration, CERN seminar, Feb. 25th, 1997.
70. M. Carena, G.F. Giudice, S. Lola and C.E.M. Wagner, *Phys.Lett.* **B395** (1997) 225.
71. W.D. Schlatter, for the LEP Working Group on Four-Jet Final States, CERN seminar, Feb. 25th, 1997.
72. G. Altarelli, J. Ellis, G.F. Giudice, S. Lola and M.L. Mangano, CERN preprint TH/97-40, hep-ph/9703276.
73. H.S. Kambara, for the CDF Collaboration, hep-ex/9706026.
74. J.L. Hewett, Proceedings 1990 Summer Study on High Energy Physics, Snowmass, Colorado.
75. J. Butterworth and H. Dreiner, *Nucl.Phys.* **B397** (1993) 3;
 H. Dreiner and P. Morawitz, *Nucl.Phys.* **B428** (1994) 31;
 E. Perez, Y. Sirois and H. Dreiner, Contribution to Beyond the Standard Model Group, 1995-1996 Workshop on Future Physics at HERA, see also the Summary by H. Dreiner, H.U. Martyn, S. Ritz and D. Wyler, hep-ph/9610232.
76. T. Kon and T. Kobayashi, *Phys.Lett.* **B270** (1991) 81;

- T. Kon, T. Kobayashi and S. Kitamura, *Phys.Lett.* **B333** (1994) 263;
T. Kon, T. Kobayashi, S. Kitamura, K. Nakamura and S. Adachi, *Z.Phys.*
C61 (1994) 239;
T. Kobayashi, S. Kitamura and T. Kon, *Int.J.Mod.Phys.* **A11** (1996)
1875.
77. D. Choudhury and S. Raychaudhuri, *Phys.Lett.* **B401** (1997) 54.
78. M. Hirsch, H.V. Klapdor-Kleingrothaus and S.G. Kovalenko,
Phys.Rev.Lett. **75** (1995) 17, and *Phys.Rev.* **D53** (1996) 1329.
79. J. Ellis, S. Lola and K. Sridhar, CERN preprint TH/97-109, hep-
ph/9705416.
80. J. Kalinowski, R. Rückl, H. Spiesberger and P. Zerwas, hep-ph/9703288.
81. M.A. Doncheski and S. Godfrey, hep-ph/9703285;
C.G. Papadopoulos, hep-ph/9703372.
82. J. Kalinowski, R. Rückl, H. Spiesberger and P. Zerwas, hep-ph/9703436.
83. LHCC Workshop on Supersymmetry,
<http://www.cern.ch/Committees/LHCC/SUSY96.html>.
84. I. Hinchliffe, F.E. Paige, M.D. Shapiro, J. Soderqvist and W.Yao,
Phys.Rev. **D55** (1997) 5520.